Faculty of applied sciences

Joachim HEINESCH

Development of a 1D model for the prediction of piano key weirs discharge capacity

Faculty of Applied Sciences - Civil engineering
Final thesis submitted in order to obtain the master degree in civil engineering

Committee's members

Sébastien ERPICUM (Uliège, Advisor)
Michel PIROTTON (Uliège, Advisor)
Julien VERMEULEN (EDF)

Academic year 2022-2023

Acknowledgments

First and foremost, I would like to express my sincere gratitude to my advisors, Prof. Sébastien Erpicum and Prof. Michel Pirotton, for their unwavering support, invaluable guidance, and exceptional supervision throughout the entirety of this endeavor.

I would also like to extend my appreciation to Vincent Schmitz, Prof. Pierre Archambeau, and Eng. Bernard Valluy for their invaluable assistance and availability.

Furthermore, I wish to extend my gratitude to the research teams at EDF, the Hydraulic Laboratory at EPFL, and the University of Liège for their collaboration, without which this work would not have been feasible. A profound thank you to Eng. Julien Vermeulen, committee member, for dedicating time to evaluate this study.

Lastly, I would like to acknowledge my family, particularly my sister Zazie, my partner Aurélie, and my grandparents Agnes and Michel, for the unwavering support they have provided me throughout this project and my academic journey.

Abstract

This master's thesis enhances a 1D flow model named WOLF1DPKW, designed to predict the discharge capacity of Piano Key Weirs (PKWs). These weirs hold paramount importance for dam safety, playing a pivotal role both socially and technologically within hydraulic infrastructures.

The model is built upon the concept of two adjacent water lines crossing the PKW, exchanging water and lateral momentum. This allows for a 1D modeling approach. Prior to any parametric optimization, the preliminary outcomes of this model necessitate refinement. Minimizing these discrepancies is the objective of this work, while maintaining a strong grounding in physics.

After a brief introduction, the second chapter presents the existing model, identifies its weaknesses, quantifies errors, and outlines ideas for potential improvements. The main avenues explored are (1) the incline of the flow axis at the inlet, (2) a modification of the lateral crest discharge coefficient, (3) an adjustment of the alpha coefficient characterizing lateral momentum exchange, and (4) a modification of the locations for lateral flux extraction and injection.

Subsequently, a sampling of the provided database is conducted to maximize the relevance of statistical analyses.

The fourth chapter showcases the outcomes of numerical simulations and the sensitivity analyses. To maintain a resolutely physics-based perspective, these results are examined using a hydraulic approach, allowing for both statistical and physical evaluation of their relevance for model enhancement.

In conclusion, the findings of this research reveal that idea 1 is not retained, as a horizontal flow axis at the inlet yields better results than an inclined axis. Idea 2 highlights the significant influence of the lateral discharge coefficient at low flow rates, but not at high flow rates, where the model error reaches a maximum. Idea 3 reflects a similar trend to 2, with divergent behaviors observed in specific geometric configurations.

Résumé

Ce mémoire de fin d'études améliore un modèle d'écoulement 1D nommé WOLF1DPKW, conçu pour prédire la capacité de débit des déversoirs en touches de piano (PKWs). Ces déversoirs revêtent une importance primordiale pour la sécurité des barrages, jouant un rôle crucial à la fois sur le plan social et technologique au sein des infrastructures hydrauliques.

Ce modèle exploite l'idée de deux lignes d'eau adjacentes traversant le PKW en s'échangeant de l'eau et de la quantité de mouvement latéralement, ce qui permet une modélisation 1D. Cette approche est propice à une analyse paramétrique, mais les résultats préliminaires de ce modèle demande à être raffinés. Minimiser ces erreurs est l'objectif de ce travail, mais avec une approche aussi ancrée que possible dans la physique.

Après une introduction rapide, le second chapitre présente le modèle existant, identifie ses faiblesses, quantifie les erreurs commises et liste des pistes d'améliorations envisagées. Les principales pistes exploitées sont (1) l'inclinaison de l'axe d'écoulement dans l'inlet, (2) une modification du coefficient de débit des crêtes latérales, (3) une modification du coefficient alpha caractérisant les échanges latéraux de quantité de mouvement et (4) une modification des lieux d'extraction et d'injection des flux latéraux.

Ensuite, un échantillonnage de la base de données fournie est réalisée pour maximiser la pertinence des analyses statistiques.

Le quatrième chapitre présente les résultats des simulations numériques et ces analyses de sensibilité. Pour conserver une perspective résolument ancrée dans la physique, ces résultats sont étudiés selon une approche hydraulique, permettant une évaluation à la fois statistique et physique de leur pertinence pour l'amélioration du modèle.

En conclusion, cette recherche révèlent que la piste n°1 n'est pas retenue, car un axe d'écoulement horizontal dans l'inlet fournit de meilleurs résultats qu'un axe incliné. La piste n°2 met en évidence l'influence importante du coefficient de débit latéral à faible charge, mais non à charge élevée, où l'erreur du modèle atteint un maximum. La piste n°3 reflète une tendance similaire à la n°2, avec des comportements divergents observés dans certaines configurations géométriques.

Contents

List of Figures

List of Tables

Chapter 1

Introduction : addressing societal challenges through weir engineering

Water management plays a crucial role in addressing various challenges faced by societies worldwide, such as flood control, efficient use of water resources, hydropower generation, and environmental conservation. Weir infrastructures, with their ability to regulate water flow, are vital components in achieving these objectives. As the demands for flood control, water resource management, and environmental preservation intensify, there is an increasing need to improve existing weirs and develop innovative designs to meet evolving requirements.

Weirs serve as critical hydraulic structures, enabling engineers to control water levels, regulate flow rates, and manage water distribution. They play a pivotal role in mitigating the impact of floods, protecting vulnerable areas, and ensuring the safety of surrounding communities. Additionally, weirs are essential for water supply management, allowing for efficient allocation of water resources among different sectors, including agriculture, industry, and domestic use.

In recent years, the challenges faced by engineers in the field of water management have grown significantly. Climate change, with its associated increase in extreme weather events, has highlighted the urgent need for improved flood control measures. Rising sea levels and changing precipitation patterns have raised concerns about the vulnerability of coastal regions and river basins to flooding. To address these challenges, engineers are required to develop robust, reliable, and cost-effective weir structures that can withstand extreme hydraulic conditions.

Moreover, the growing demand for renewable energy sources and the transition towards a low-carbon economy have placed hydropower generation in the spotlight. Dams and their weirs, serving as important structures in hydropower projects, play a crucial role in regulating the flow of water and ensuring the safety and stability of hydroelectric facilities. As the need for clean energy intensifies, engineers are faced with the task of designing weirs that not only optimize energy production but also minimize environmental impacts and efficiently manage

water flow during flood events.

In parallel, the importance of environmental conservation and the preservation of aquatic ecosystems cannot be overstated. Dams have a direct impact on the natural flow regime of rivers and streams, affecting the habitats of various species and the overall ecological balance. To ensure the sustainability of water management practices, engineers must strive to design weirs that are not only efficient in their primary functions but also considerate of environmental concerns. This involves maintaining adequate fish passage, preserving water quality, and mitigating the disruption of natural habitats.

In light of these pressing challenges and evolving societal needs, the development of improved numerical studies for weir structures becomes paramount. Numerical modeling provides engineers with a powerful tool to analyze and optimize the design and operation of weirs. By accurately simulating the hydraulic behavior of weirs, engineers can gain insights into flow patterns, evaluate structural performance, and identify potential areas for improvement.

This master's thesis aims to contribute to the advancement of weir engineering by focusing on the development of a numerical model specifically targeting Piano Keys Weirs (PKWs). PKWs, known for their unique geometric configuration and hydraulic efficiency, offer promising solutions for flood control, hydropower generation, and environmental preservation. However, to fully harness the benefits of PKWs, it is essential to develop better numerical models that accurately capture their hydraulic behavior and provide reliable predictions.

By enhancing existing numerical codes and minimizing empirical calibration, this thesis strives to develop a physically-based numerical model for PKWs that can be validated against a comprehensive dataset. The objective is to provide engineers with a robust and versatile tool for optimizing PKW designs, evaluating their performance under various hydraulic conditions, and ensuring their effectiveness in real-world applications.

Through this research, we aim to support the global efforts towards improved weir infrastructures that enhance flood control measures, optimize water resource management, facilitate sustainable hydropower generation, and uphold high standards of environmental conservation. By advancing the knowledge and understanding of PKWs and their hydraulic behavior, we contribute to the ongoing quest for more efficient and resilient water management solutions.

Chapter 2

State of the art : from weirs to PKW 1D modeling

1 Overview of weir infrastructures

In this section, a comprehensive understanding of weirs and the existing technological solutions employed in water management projects will be presented. Subsequently, various types of weirs, including the classical ones, will be discussed as they serve as the foundation for the design and analysis of the piano key weir, which constitutes the main focus of this study. In addition, this section will facilitate a brief comparative analysis of weir geometries, highlighting the advantages of the piano key weir design.

1.1 Weirs within hydraulic structures

Weirs are critical components within hydraulic structures, working in conjunction with dams and spillways to regulate water flow and manage water distribution. A dam is a barrier constructed across a river or a stream, primarily designed to store water and create a reservoir. Spillways, on the other hand, are structures incorporated into dams to provide controlled release of excess water, maintaining the reservoir at a safe level during periods of high inflows or flood events.

As shown in Figure 2.13, excess water can sometimes be retained by a gate and then flows over the weir, where the geometry determines the amount of water that can pass through. It then gains velocity over the downstream channels. Finally, its energy is dissipated on the energy dissipation structure (in this case, a ski jump) to join the downstream flow while minimizing environmental impacts.

Weirs, within the context of hydraulic structures, serve multiple purposes. They enable engineers to control water levels by diverting flows over their crest, regulate flow rates by adjusting the effective weir length, and manage water distribution among different outlets or downstream

channels. Weirs play a pivotal role in mitigating the impact of floods, protecting downstream areas, and ensuring the safety of communities located along the river.

Figure 2.1: Downstream view of the Bort-les-Orgues dam and its gated weir

1.2 Technological solutions for spillways

A variety of technological solutions exist for the design and construction of spillways. These solutions encompass different geometries, operational mechanisms, and flow control features. The selection of a specific spillway type depends on factors such as the anticipated flow rates, the topography of the site, available resources, and project requirements. Those factors will have a direct impact on the design of the weirs.

1.3 Geometric design of weirs [1]

The geometric configuration of weirs significantly influences their hydraulic performance. Various shapes and profiles have been employed to optimize flow characteristics and ensure efficient water management. Here are the most common geometric designs.

Sharp-crested weir

The basic shape of weir is the so called sharp-crested weir. It consists in a thin vertical wall placed transversally to the main flow.

Figure 2.2: Flow over a sharp-crested weir

Its discharge capacity can be calculated from the traditional Poleni equation:

$$Q = C_{dW} W \sqrt{2gH^3} \tag{1.1}$$

where Q is the discharge passing over the structure, W is the crest length, H is the water head upstream the weir calculated as the sum of the water depth over the crest and the kinetic energy component, and CdL is a discharge coefficient approximately equal to 0.429 for sharp-crested weirs.

The discharge coefficient value is slightly dependent of the weir thickness and height.

Broad-crested weir

A thick-crested weir is called broad-crested one as long as its thickness is sufficient to enable the development of a critical water depth hc over the crest. This is the case if the H/T ratio is lower than 0.5 [2]. The discharge coefficient C_{dW} for broad-crested weirs is equal to 0.385.

Figure 2.3: Flow over a broad-crested weir

Ogee-crested weir

The ogee-crested weir is actually the most used weir in large-scale water management projects. Its shape follows the trajectory of the free nappe observed on a sharp-crested weir for the design head (Figure II-3). The discharge coefficient for the design head is equal to 0.494.

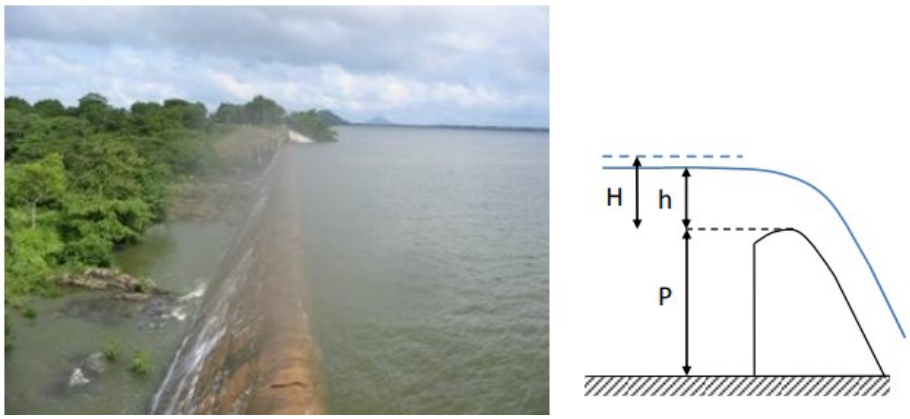

Figure 2.4: Flow over an ogee-crested weir

As this weir seems to be the optimal design for linear free weir, it is commonly used as a reference to compare the various weir geometry efficiencies.

Side weir

The side weir is a linear weir placed parallel to the main flow direction (Figure 2.5). Its discharge capacity is thus affected by the variation of flow depth along the weir, the flow velocity and the outflow angle [3].

Figure 2.5: Flow over a side weir

Labyrinth weir

The labyrinth weir is a multi linear thick crested weir (Figure 2.6). Using trapezoidal horizontal scheme, it enables to increase the crest length L for a given weir width W.

Figure 2.6: Flow over a labyrinth weir

Piano key weir

The Piano Key Weir (PKW) is a particular shape of labyrinth weir, using up- and/or downstream overhangs (Figure 2.12). The horizontal rectangular labyrinth shape allows to multiply the crest length for a given weir width. As the labyrinth weir, the PKW is so a strong solution for dam projects needing a high specific discharge capacity or with low reservoir section allocated to the flood discharge. Furthermore, the use of overhangs limits the footprint of the structure. The PKW could thus be placed directly on dam crest, what makes it a useful tool for dam rehabilitation.

Figure 2.7: Piano Keys weir

Figure 2.8: Flow over the piano keys weir of Campauleil, France

The PKW was firstly designed in 2001 by Lempérière [4], from the non-governmental organisation "Hydrocoop", who was searching for a weir shape efficient and easy to build for

development projects all over the world. He looked for a shape allowing a large specific discharge capacity, for the use of precast elements and for a design based on a single parameter. This goal was finally achieved and developed in [5]. The first PKW has been built in 2006 for the Goulours dam rehabilitation by "Electricité de France (EDF)" [6]. Since this time, EDF developed several projects of PKW for dam rehabilitation in France [7][8][9][10][11][12][13][14][15][16]. Since 2010, PKW is also studied for new dam projects in Asia [17][18][19][20] and in Africa [11][13][21][22][23].

1.4 Comparative study

The discharge capacity can be derived by utilizing the well-established Poleni equation, as discussed previously (Equation 1.1). To facilitate a comparative analysis of the discharge capacity across various weir configurations and contextual scenarios, we can employ a non-dimensional coefficient derived from the aforementioned equation:

$$C_{dL} = \frac{Q}{L\sqrt{2gH^3}} \tag{1.2}$$

where Q is the discharge passing over the structure, L is the crest length (not the developed crest length), H is the water head upstream the weir calculated as the sum of the water depth over the crest and the kinetic energy component.

Despite the existence of various corrective equations proposed by several authors to account for factors such as relative height, effective crest length, and weir thickness, among others, an encompassing analysis can be found in Table 2.1. This table provides a comprehensive overview of the theoretical discharge coefficients, highlighting their potential range of variation and offering a comparative assessment of their efficiency against the discharge coefficient of an ogee-crested weir at its design head.

Weir geometry	C_{dL}	$C_{dL}/0.494$
Sharp-crested weir (theoretical)	0.429	0.87
Broad-crested weir (theoretical)	0.385	0.78
Ogee-crested weir at design head	0.494	1
Ogee-crested weir	$0.385 - 0.6$	$0.78 - 1.2$
Labyrinth weir	Up to 0.8	Up to 2
Piano key weir	Up to 2.5	Up to 5

Table 2.1: Coefficient discharge of different types of weirs - comparative study

As the discharge capacity is directly proportional to the weir crest length, the ratio between labyrinth or piano key weir and sharp-crested weirs efficiencies should reach the value of the L/W ratio. This is true for low upstream heads. This advantage made of the labyrinth and PKW strong solutions for dam projects needing a high specific discharge capacity or with low

reservoir section allocated to the flood discharge.

However for increasing heads, their discharge capacity decrease due to nappe interactions [24]. Furthermore, as parts of the crest are not perpendicular to the main flow direction, the crest efficiency decreases with the direction of the flow compare to the orientation of the walls.

Furthermore, due to its structural properties, it can be easily installed on existing installations, allowing for cost-effective enhancement of safety levels. With its alternating slopes between each "piano key," it facilitates flow separation. The flow on the ascending slope is projected before joining the flow on the descending slope. This design feature enhances energy dissipation, thereby reducing the sizing requirements of downstream dissipation structures.

Hence, the PKW presents a technological solution that proves to be more cost-effective in meeting dam safety requirements in numerous rehabilitation and new construction projects.

2 The Piano Keys Weir - Nomenclature

The PKW geometry involves a large set of parameters. In order to ensure a unicity in terminology, a naming convention has been developed by a workgroup gathering “EDF-Hydro Engineering Center”, “Ecole Polytechnique Fédérale de Lausanne - Laboratory of Hydraulic Constructions” and “University of Liège - Laboratory of Hydraulics in Environmental and Civil Engineering (HECE)” [25].

The basic structure is composed of “PKW units”. The parameters relying to the basic structure are the total width of the PKW W, the total developed crest length L and the number of PKW units constituting the structure N_u.

The unit represents the smallest extent of a complete structure, composed of an entire inlet key with two side walls and half an outlet on both sides. The parameters dedicated to the PKW unit are defined with an index u, when the ones dedicated to the inlet key, the outlet key and the side wall are respectively defined with indexes i, o and s. The main parameters defining the geometry of the PKW unit are the unit width W_u, the inlet and outlet keys widths W_i and W_o, the inlet and outlet keys heights P_i and P_o, the slopes of the inlet and outlet keys S_i and S_o, the up- and downstream overhangs lengths B_o and B_i, the upstream-downstream PKW length B, the base length B_b, and the crest thickness T_x with x index equal to i for the crest downstream of the inlet key, o for the upstream crest of the outlet key and s for the crest on the side wall (Figure 2.9).

As the PKW is mainly used on dam crest, the dam height under the weir P_d has to be characterized.

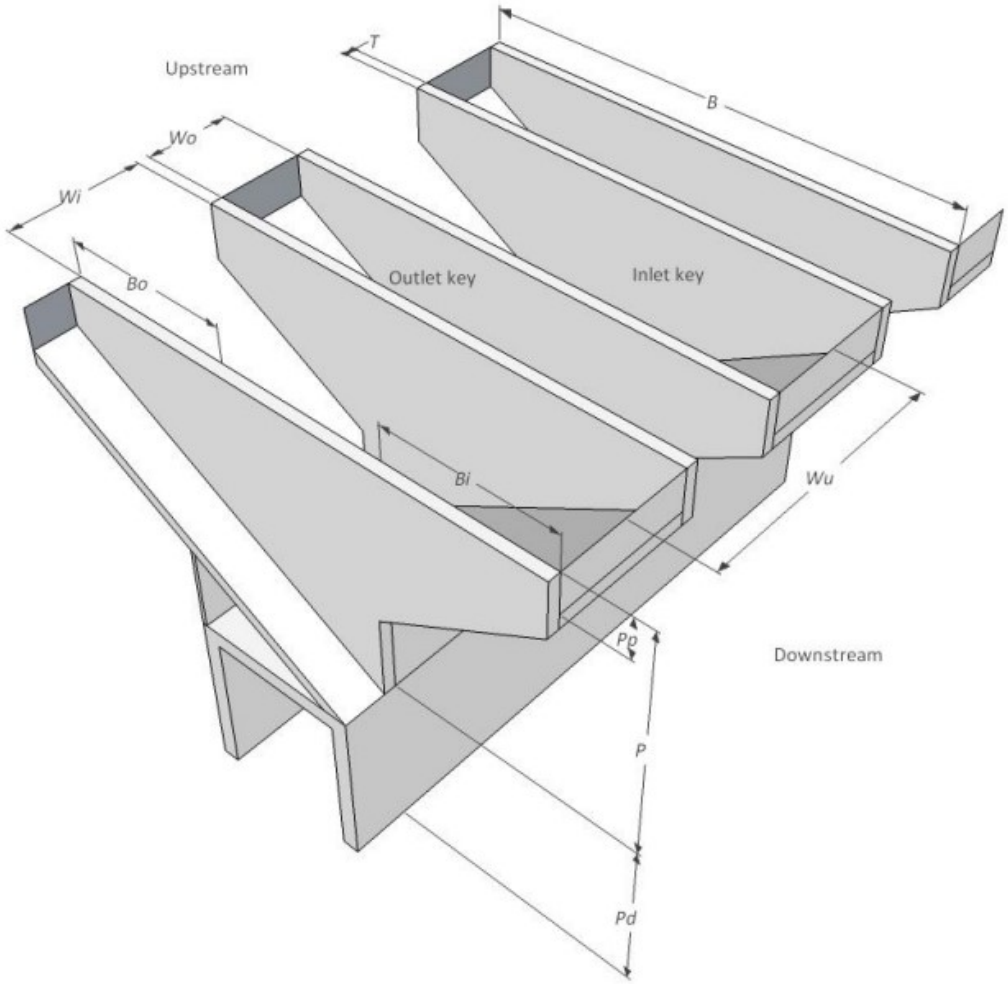

Figure 2.9: 3D Sketch of the basic structure of a PKW and its main geometrical parameters

3 PKW modeling : Wolf1DPKW, an existing model to improve

3.1 Introduction

By offering a thorough exposition of the model's framework and underlying principles within this chapter, readers will acquire a robust comprehension of its fundamental groundwork, thereby facilitating a more targeted examination of the subsequent chapters' advancements and enhancements.

It is important to note that while this chapter provides a comprehensive overview, most of the following developments were extensively documented before [26]. This article and development in annexes serve as valuable resources, offering in-depth explanations and analyses of the specific methodologies, algorithms, and experimental validations employed to improve the model's performance and accuracy.

3.2 A global overview

The overall structure of the code can be depicted using Figure 2.10 as a schematic representation.

3.3 Principles

A PKW can be conceptualized as the repetition of n identical elements, each composed of an inlet and an outlet, referred to as a "PKW-unit." As each of these units exhibits symmetry, the study primarily focuses on the numerical modeling of the flow on a half-inlet and half-outlet, referred to as a "PKW-element." The overall flow traversing the entire structure can then be estimated by assuming symmetrical flow within each PKW-unit and identical flow across all PKW-units. While this assumption is challenged by the actual approach conditions, it is commonly employed due to its computational efficiency, accurate results, and the current inability to consider unique approach conditions for each project at this phase of analysis.

"*According to experimental observations [27] [28], the main flow direction in the outlet follows the bottom slope. Consequently, the x-axis has been locally inclined in the numerical model. It is not the case in the inlet where the main flow direction is rather horizontal. The x-axis has thus been directed horizontally along the inlet (Fig 2.11)*" [26].

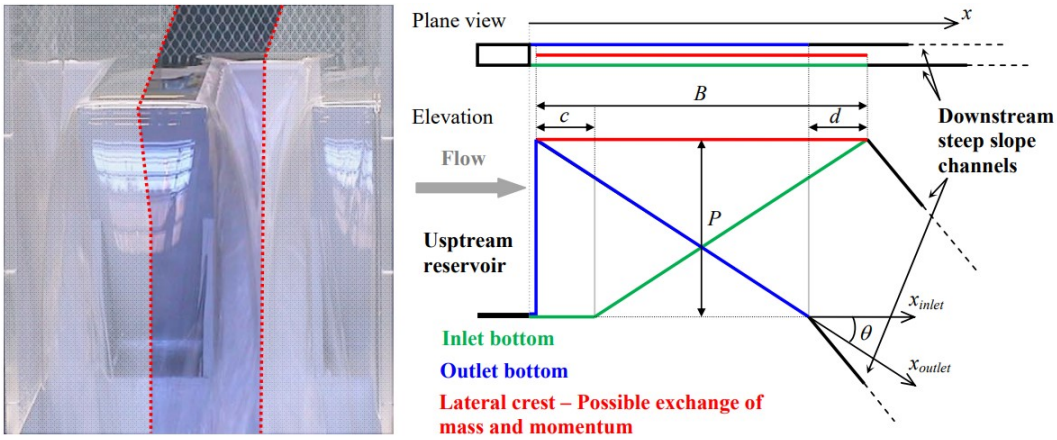

Figure 2.11: Basic element of a PKW (left) and numerical model layout with main geometric parameters (right)[26]

"*The geometric paramaters needed to set up the numerical model are the dam height under the weir P_d, the inlet and outlet keys heights P_i and P_o, the upstream-downstream PKW length B, the up- and downstream overhangs lengths B_o and B_i, the PKW unit width W_u and the inlet channel width $W_i/2$ and the outlet channel one $W_o/2$*" [26].

3.4 Mathematical model

Governing equations

"*The flow model is based on the one-dimensional cross-section-averaged equations of mass and momentum conservation. In this standard 1D approach, it is basically assumed that velocities normal to the main flow direction are significantly smaller than those in this main flow direction. Consequently, the pressure field is almost hydrostatic everywhere and the free surface is horizontal along the transverse direction*" [26].

"*The conservative form of the governing equations can be written as follows, assuming a rectangular cross-section of constant width:* " [26]

$$\begin{aligned} \frac{\partial A}{\partial t} + \frac{\partial Q}{\partial x} &= q_l && \text{Mass conservation} \\ \frac{\partial Q}{\partial t} + \frac{\partial (uQ + \frac{1}{2} g \cos\theta L h^2)}{\partial x} &= \left(-g \cos\theta A \frac{\partial z_b}{\partial x} + g\ A \sin\theta\right) - \frac{\tau_{bx}}{\rho} + \alpha u q_l && \text{Momentum equation} \end{aligned} \tag{3.1}$$

where "*t is the time, x the space coordinate, Ω the cross-section, Q the discharge, h the water depth, u the cross-section-averaged velocity, L the section width, z_b the bottom elevation, g the gravity acceleration, Θ the inclination of x-axis, ρ the density of water, τ_{bx} the bottom shear stress, q_l the lateral unit discharge and α a coefficient $[0, 1]$ quantifying the change in momentum because of the lateral discharge*" [26].

Grid and numerical scheme

Firstly, due to the choice of 1D modeling, both channels representing the inlet and outlet are assumed to have a rectangular cross-section along their entire length. While this strong assumption holds relatively true for a portion of the domain, it does not accurately represent the situation near the overhangs. Therefore, the spaces beneath these overhangs are neglected, and the topography upstream of the outlet is replaced with a "step". Downstream, including downstream of the inlet where the issue of space beneath the overhang arises, a steep slope of the bed is imposed (45°) to induce a supercritical flow. This assumption, which is less strong since PKWs are typically placed on top of existing structures ($P_d \neq 0$), introduces a more significant topographic step that generally results in a supercritical flow. No downstream boundary condition is required, and this fictitious slope also addresses the issue of spaces beneath the downstream overhangs. Those assumptions on the topography are illustrated in Figures 2.12 and 2.13.

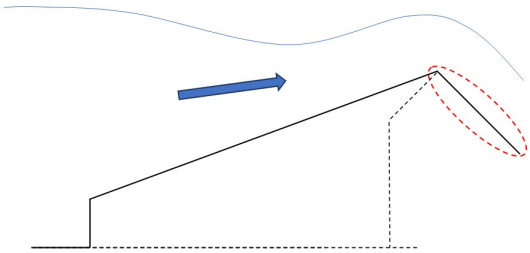

Figure 2.12: Inlet topography - reality vs model

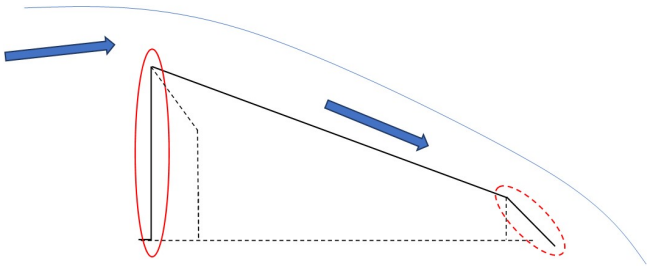

Figure 2.13: Outlet topography - - reality vs model

"*The space discretization step dx in both channels is constant* (according to a horizontal axis) *[...] This enables a direct computation of the lateral exchanges mesh by mesh without interpolation of the flow variables. [...] The discretization in space is done with a finite volume scheme for handling properly discontinuous solutions*" [26].

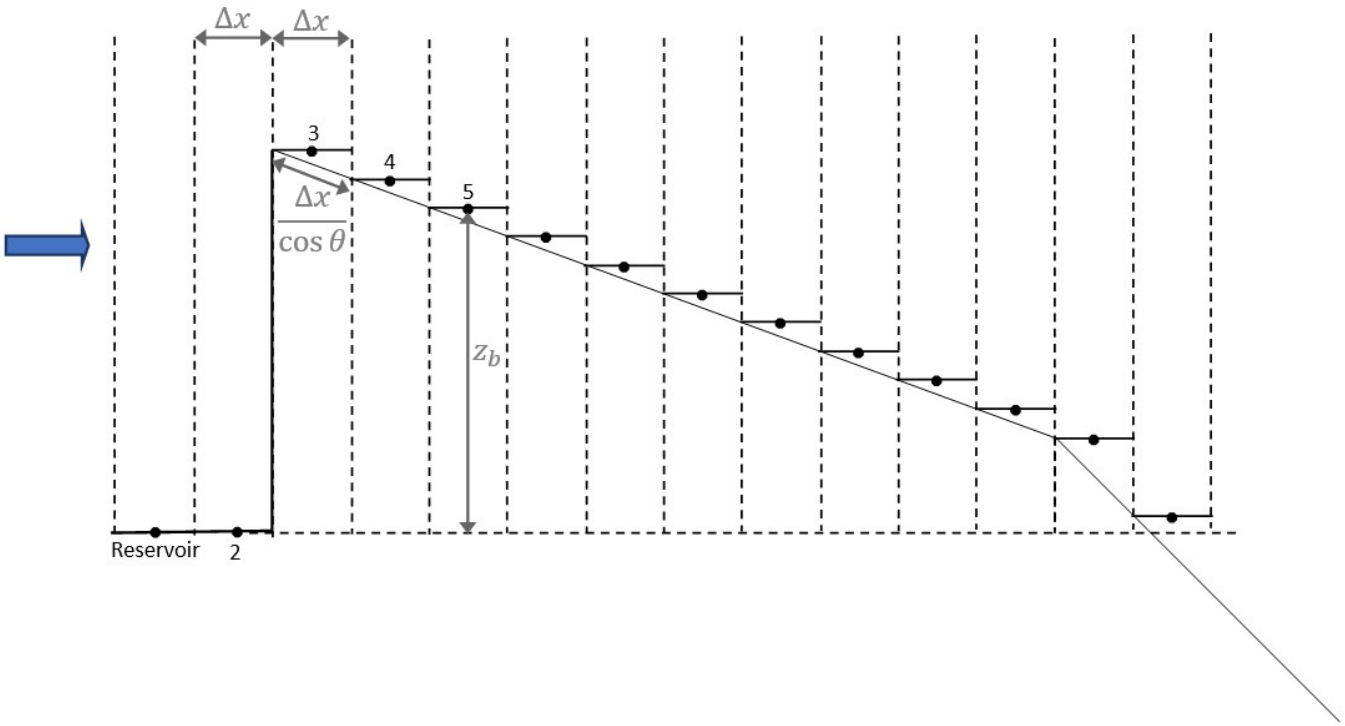

Figure 2.14: Discretization with finite volumes of an outlet - finite volume boarders and location of the unknowns

Figure 2.14 serves as an example to illustrate the discretization of an "outlet." To accurately maintain the weir height and because of the continuous reconstruction in flux calculations, the unknown bed elevation at a given cell, that remains fixed throughout the simulation, corresponds to the upstream bed elevation of the finite volume (upstream in relation to the reservoir, not with respect to the flow within the finite volume). Additionally, this figure highlights that when the main flow axis is inclined, the width of the finite volume in the inclined section is no longer Δx but rather $\Delta x / \cos\Theta$, with Θ the angle between the horizontal and the main flow axis.

The evaluation of the fluxes (space derivatives) are "*simply dictated by the sign of the flow velocity reconstructed at the cells interfaces*" [26] [29] [30] [31] [32]. The model uses a constant reconstruction of the variables. The fluxes Q and uQ are evaluated with the unknown located in the center of the upstream finite volume. We use the downstream unknowns to evaluate the flux $0.5g\cos\theta Lh^2$.

Source terms

According to the flux evaluation, a suitable treatment of the topography gradient source term is a downstream discretization of the bottom slope and a mean evaluation of the corresponding water depths [33] [31] [34]. For a cell i, the bottom slope discretization writes:

$$-g\cos\theta\ \Omega\frac{\partial z_b}{\partial x}\bigg|_i \quad \Rightarrow \quad -g\cos\theta\frac{(\Omega_{i+1}+\Omega_i)}{2}\frac{(z_{bi+1}-z_{bi})}{\delta x} \tag{3.2}$$

where subscript $i+1$ refers to the downstream cell along x-axis.

As it is not entirely suited regarding water in movement over an irregular bed, on the upstream side of the outlet channel (finite volume 2 and 3 in FIGURE 2.14), i.e. where the topography gradient is locally the most important, the momentum equation has been locally replaced by the energy equation [33].

"*The bottom friction is conventionally modeled with the Manning formula, where the Manning coefficient n characterizes the surface roughness and R is the hydraulic radius* :

$$\frac{\tau_{bx}}{\rho} = \frac{gn^2 Au|u|}{R^{4/3}} \quad \text{with} \quad R = \frac{\Omega}{\Psi} = \frac{A}{L+h'} = \frac{A}{L + \min\left(h, z_{\text{lat weir}} - z_b\right)} \tag{3.3}$$

where z_s is the lateral weir elevation, to take into account the reduced width of the inlet and the outlet" [26].

"*Finally, the lateral unit discharge in the lateral exchange terms was, before the code updates, computed on each point of the lateral weir depending on the head difference ΔH between the inlet and the outlet, without considering the kinetic terms along the inlet and outlet axis* :

$$\begin{gathered} q_l = \mu\sqrt{2g\left|\Delta H\right|^3}\ \text{sign}\ q(\Delta H) \qquad q_{l_{in}} = q_l \qquad q_{l_{out}} = -q_l \\ \Delta H = \max\left(0\ ,\ z_{bin} + h_{in} - z_{\text{lat weir}}\right) - \max\left(0\ ,\ z_{bout} + h_{out} - z_{\text{lat weir}}\right) \end{gathered} \tag{3.4}$$

where μ is the lateral weir discharge coefficient and subscripts in and out refer respectively to the inlet and the outlet channel" [26].

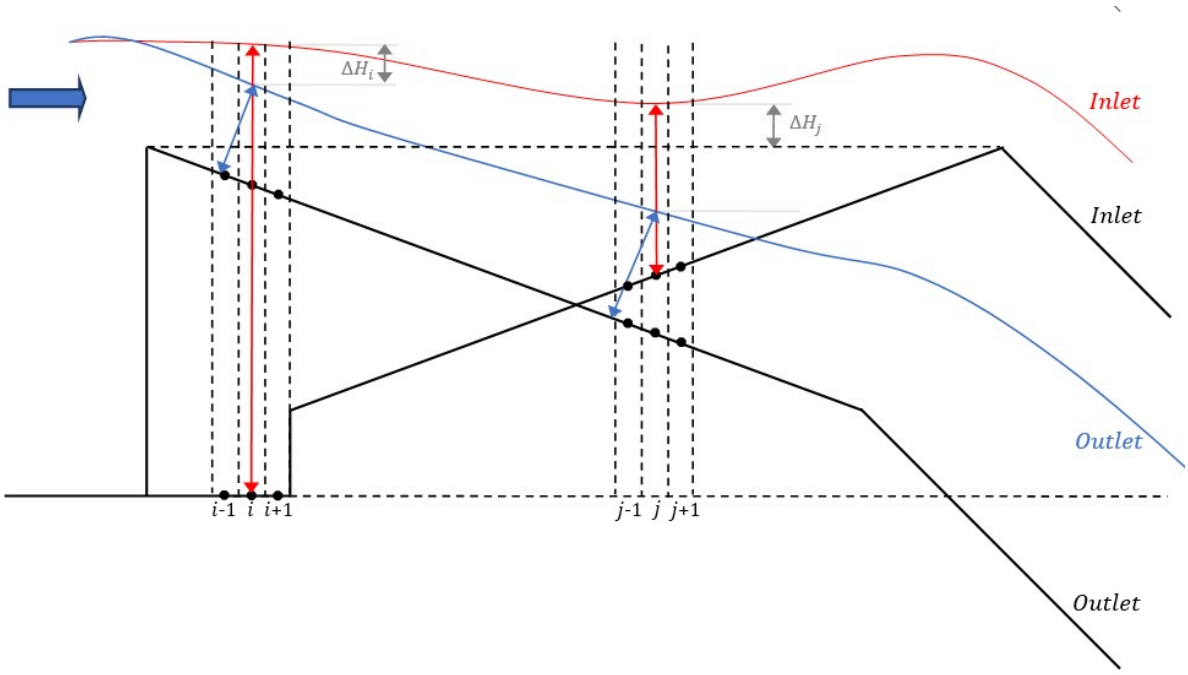

Figure 2.15: Calculating lateral fluxes based on free surfaces expressed in different reference frames.

As depicted in Figure 2.15, when considering different 1D flow inclinations for the inlet and outlet, it becomes necessary to make an assumption regarding the computation of the head difference between the two channels. Additionally, the locations for lateral flow extraction within the inlet and re-injection within the outlet need to be determined. In the existing model, the free surface is represented in a horizontal-vertical reference frame for calculating water height differences. This difference corresponds to the head difference, as no kinetic component is accounted for. The discharge is then extracted and reintroduced into the control volumes, with their center of gravity located at the same horizontal abscissa as where the head difference is computed.

Upstream reservoir

The upstream reservoir distributes the discharge between the inlet and the outlet channel.

It is modeled as two special twin 1D finite volumes, with distinct discharges $Q_{R,out}$ and $Q_{R,in}$ but a single cross-section value Ω_R. Assumptions made in this model are that the discharge distribution is directly proportional to the widths of both the inlet and outlet, and that the source terms are neglected in these particular twin finite volumes. The procedure to model the reservoir is very close to the ones developed by the authors to link 1D and 2D models or to perform 2D multiblock – multimodel modeling [30] [26] [31] [35].

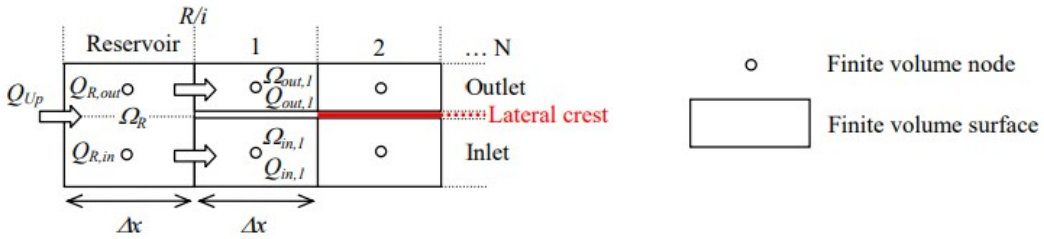

Figure 2.16: Modeling of the upstream reservoir and links with the inlet and the outlet [26]

The value of the head on the PKW will be calculated in this twin finite volume to define the release efficiency of the structure.

Boundary conditions

As detailed before, "*the steep slope of both channels in the downstream part of the model leads to supercritical flow and no outflow boundary condition is thus needed*" [26]. Thus, the value of the upstream discharge is the only value to be prescribed as a boundary condition.

Time discretization

"*Since the model is applied to compute steady-state solutions, the time integration is performed by means of a 3-step first order accurate Runge-Kutta algorithm, providing adequate dissipation in time. For stability reasons, the time step is constrained by the Courant-Friedrichs-Levy condition based on gravity waves. A semi-implicit treatment of the friction term is used, without requiring additional computational costs.*

Slight changes in the Runge-Kutta algorithm coefficients allow modifying its dissipation properties and make it suitable for accurate transient computations" [26].

Other features

"*With a typical space step of 5 mm to model standard experimental PKW 50 cm long and 10 cm wide, the computation of the flow over the structure takes less than 2 min on a desktop computer*".

"*A convergence criteria has been defined on the basis of the discharge evolution in the reservoir ($Q_{R,in} + Q_{R,out}$) compared to the upstream discharge boundary condition. When the difference between both values is lower than a given tolerance during a fixed time, the computation is assumed to be converged*" [26].

3.5 Previous accuracy

"The numerical results are in satisfactory agreement with the experimental ones in a large part of the CwH/P curve, especially for moderate head ratios (Figure 2.17). The numerical curve shape is similar to the experimental one. For large and very small head ratios, the efficiency of the PKW is systematically overestimated by the numerical model." [26]

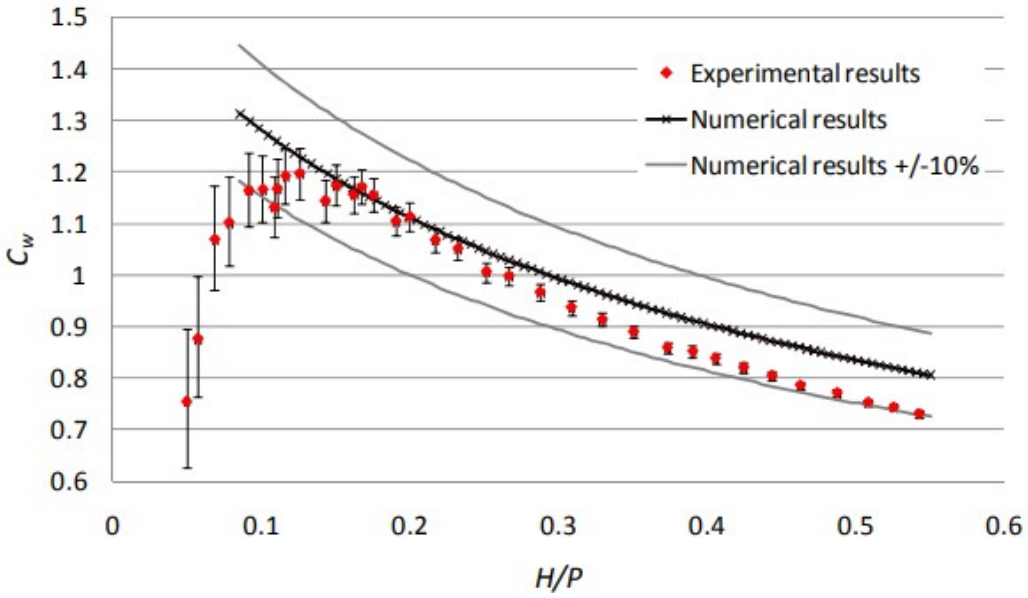

Figure 2.17: *"Comparison of experimental and numerical results - Release capacity of the PKW"* [26]

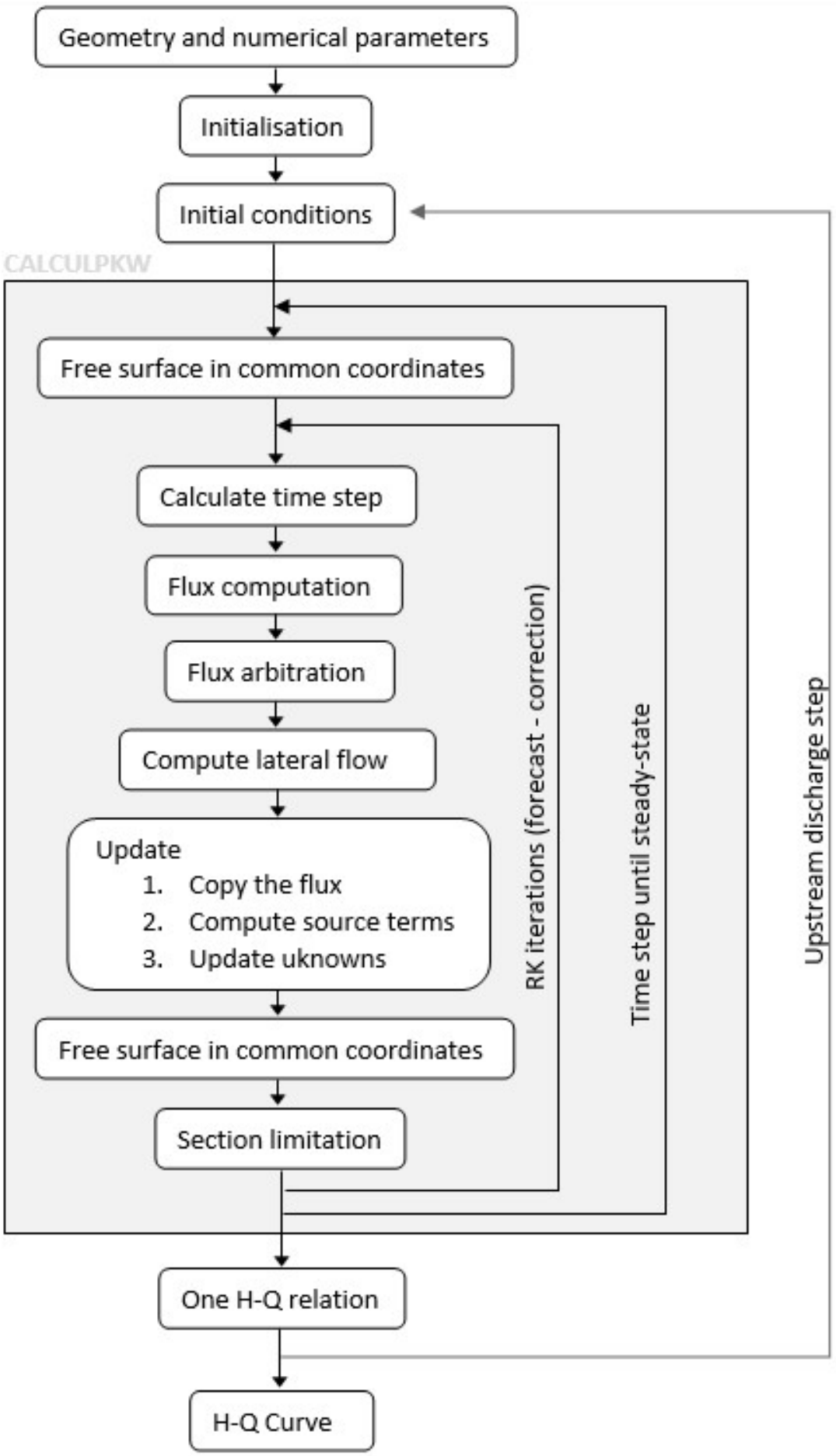

Figure 2.10: Global structure of WOLF1DPKW

4 Experimental data

4.1 Introduction

This chapter provides an overview of the database utilized in this research, which contains valuable information for the validation and analysis of the developed code. The database consists of 113 configurations of Piano Key Weirs (PKWs), encompassing various geometrical parameters and corresponding discharge capacity measurements. The collaboration between three prominent institutions, namely Uliège University, EPFL (École Polytechnique Fédérale de Lausanne), and EDF (Electricité de France), has resulted in the establishment of a comprehensive and diverse dataset.

4.2 Database Contents

The database encompasses detailed information for each PKW configuration, including geometrical parameters and discharge capacity measurements. Specifically, the following parameters are recorded for each configuration:

- Inlet height P_i ;
- Outlet height P_o ;
- Dam heigh below the weir P_d ;
- PKW width W and number of units N ;
- Crest shapes (Broad/Round) and curvature R_i ;
- Crest thickness T_s ;
- Unit width W_u ;
- Inlet width W_i ;
- Outlet width W_o ;
- Length of lateral crest B ;
- Upstream overhang length B_o ;
- Downstream overhang length B_i.

Moreover, the discharge capacity measurements, represented by a collection of head-discharge data points, are available for all configurations $(H - q)$. In total, the database contains 1,971

charge-discharge measurements.

A complete list of geometric dimensions for these reduced-scale models is provided in the Appendix. This list contains 6 fewer configurations than the list provided by the academic team. Out of these :

- 4 configurations are found to be duplicates (having the same values of H and q);
- 1 configuration is not defined unambiguously ("Pd = 0.1-0.5m");
- configuration is duplicated with one of its corresponding measurement series showing aberrations compared to neighboring configurations.

The compilation of this extensive database is the result of fruitful collaboration between Uliège University, EPFL, and EDF. Each institution contributed its expertise and resources to collect and provide valuable data from reduced-scale physical models of PKWs. The collaborative nature of this project has ensured the inclusion of a wide range of PKW configurations, offering a comprehensive and diverse dataset for analysis and validation purposes.

4.3 Evaluation of the former database relevance

The available data is primarily used to provide an aggregated error information across the entire database. However, this information is influenced by the composition of the database itself. For instance, a configuration that has been tested multiple times with slight geometric variations, having limited impact on the values of H and Q (e.g., height below the threshold Pd), receives higher weight. The same applies to a configuration for which a particularly large number of H and Q measurements have been taken.

This information is detailed based on the originating laboratory (ULg, EPFL, EDF) since, despite the diversity of tested configurations, a certain homogeneity within each subset of data is observed (crest shapes, values of certain geometric dimensions, etc.). Furthermore, existing discharge formulas have been calibrated on these subsets, so their performance on the complete set is also representative of the significance of the corresponding subset within the database.

The majority of geometries in the database (44%) are configurations tested by EPFL. However, the density of measurements taken on ULg geometries is 3 to 4 times higher than those on EPFL and EDF geometries. In terms of "useful" measurements ($H > 0.03m$), there is an average of 30 measurements per ULg configuration, compared to 7 to 8 measurements per EPFL or EDF configuration. For lower loads, surface tensions dominate, and the results cannot be scaled. Consequently, ULg geometries (accounting for 67% of the useful measurements) have

significantly greater weight than EPFL (21%) and EDF (12%) geometries.

In order to assess the impact of this over-representation, Figures 2.21 and 2.22 illustrate the diversity of geometries and their corresponding stage-discharge relationships. These figures highlight that the University dataset covers a wide range of geometries, resulting in a broad spectrum of stage-discharge relationships compared to the overall available data. Similar observations can be made for the EPFL dataset. However, the EDF models appear to consistently exhibit less favorable discharge coefficients.

NB : In addition to the discharge measurements, surface elevation measurements are available for a number of ULg configurations, both in the inlet and outlet sections. Furthermore, a study has been published that includes a comprehensive set of flow observations on the reduced-scale models from Uliège, accompanied by a collection of photographs illustrating physical phenomena such as nappe detachment, streamline patterns, and free surface behavior [1]. These images contribute to a better understanding of the studied flow. Therefore, select photographs will be included in this work to provide a visual representation of the phenomena underlying certain numerical results.

5 Weaknesses of the model

The comprehensive analysis presented in this section is of paramount importance as it enables the identification of assumptions that may influence the accuracy of the results and provide opportunities for enhancement in the context of a 1D model. By thoroughly examining the range of assumptions employed, this investigation will help to assess their impact on the model's performance and potential limitations. Moreover, it will serve as a basis for identifying key areas where refinements and improvements can be implemented, ultimately contributing to the overall quality and reliability of the 1D model.

5.1 1D modeling

Firstly, it is always important to acknowledge the limitations of a 1D model. All 1D models, including the one presented here, assume a predominant flow direction with negligible velocity components perpendicular to the flow axis. The only exception is for the "infiltration" terms, which represent mass and momentum sources of sinks associated with flow entering or leaving the main flow. However, these inflows/outflows do not affect the assumed hydrostatic pressure distribution and the assumption or uniform speed across the width of each channel. Observations from real-world applications and physical model studies demonstrate that flow over these structures is three-dimensional. Therefore, while this 1D model serves its purpose as a useful tool, it is important to recognize that the assumption of a 1D model is a strong one.

Consequently, parallel studies on 3D numerical modeling are being conducted alongside this work, which may provide refinements that the 1D model alone cannot achieve.

5.2 Inclination of the main flow

Secondly, the choice of predominantly unidirectional flow still leaves room for selecting the direction of this flow. While we maintain the assumption of negligible lateral velocities (or captured by lateral exchanges), there remains the choice of the inclination of the flow axis with respect to the horizontal and the inclination of the channel bottom. Currently, the flow is assumed to be horizontal upstream of the PKW, horizontal throughout the entire inlet channel, and inclined according to the bottom topography in the outlet section starting from the upstream overhang.

Experimental studies show that this choice does not reflect the physical reality for the inlet section. While the flow near the free surface is predominantly horizontal, the deeper flow tends to align with the inlet topography as it rises along the upstream slope, supplying the lateral discharge at the end of the inlet and the discharge passing through the downstream crest of the inlet. Thus, improving the inclination of the flow axis in the inlet section became one focus of this study.

5.3 Infiltration source term - mass and momentum equation

Furthermore, lateral inflows, or so-called "infiltration" terms, allow us to bypass the assumption of strictly unidirectional flow without any velocity component perpendicular to the flow direction. However, this does not alter the assumptions made regarding the uniformity of velocities within the cross-section or the resulting pressure distributions. Rather, these terms enable the consideration of mass or momentum inputs or withdrawals resulting from lateral flow velocities. Thus, the inlet and outlet can exchange flows despite the absence of lateral velocities in the model.

The lateral source term in the mass equation is based on a discharge calculated using lateral spillway theory, where the difference in water height between the free surfaces in the inlet and either the free surface of the outlet channels at a common abscissa either the crest is taken as the head difference. This lateral discharge is then extracted from and re-injected into the finite volumes of the inlet and outlet located at that abscissa. The discharge coefficient, $C_{w,lat}$, is assumed to be 0.385 for unprofiled weirs (corresponding to a broad-crested weir) and 0.42 for profiled weirs (corresponding to a sharp-crested weir).

The lateral source term for momentum is expressed as a fraction (alpha) of the momentum along the main flow axis (Equation 3.1), carried by the lateral discharge: $S_l = \alpha u_x Q_l$.

While this modeling approach has several weaknesses, there is potential for improvement.

Firstly, the lateral discharge coefficient could be further refined. Several authors provide corrections based on variables such as crest thickness, relative height, degree of curvature in the case of rounded crests, etc [3].

Next, the assumption regarding the location of mass extraction and injection can be questioned. For PKWs with high relative heights (high P/W_u ratio), the slopes of the inlet and outlet channels are significant. As shown in Figure 2.15, the inclination of the flow axis in the outlet and, in improved versions of the code, in the inlet, which is proportional or equal to these channel slopes, is also substantial. As a result, the free surface, calculated as a water level perpendicular to the flow axis, can be significantly distant from the abscissa of the finite volume cell that generated it. Choosing to inject these mass and momentum flows into the cells that form the basis for calculating the free surface, rather than simply at the abscissa of the calculated free surface, could be an interesting improvement.

Moreover, in some conditions, this lateral flow can be projected from the inlet towards the outlet. This momentum can result in the lateral discharge reaching a location downstream of its initial point of entry, especially if the lateral flow exhibits high velocities along the main flow axis when passing over the crest.

Considering the challenges encountered when dealing with the inclined inlet, it becomes apparent that the inclination of the inlet can lead to conflicts in the calculation of the free surface, as different control volumes may yield different free surface elevations for the same horizontal abscissa. Resolving this data conflict is also an assumption discussed in this report.

Regarding momentum exchanges associated with infiltrations, the coefficient alpha introduces challenges in terms of calibration and reflection. Does lateral flow transport momentum along the main flow axis? If so, how much momentum? The answer is not simple as it depends on the orientation of the flows as they pass over the crest, which can induce both an increase in head due to the chute and a loss of head due to the impact of the jet when it reaches the other channel. Observations show that the dynamics of these exchanges strongly depend on the flow rate and appear to vary from upstream to downstream on the PKW, and the head change is influenced by various geometric parameters.

In the initial version of the code, lateral exchanges are assumed not to impact the main flow, which is achieved by endowing the lateral flow with the same momentum per unit mass as the flow from which it is extracted or the flow into which it is injected (Equation 5.2). However, this assumption may not fully represent the complex dynamics of momentum exchanges in the PKW. Further investigations are needed to better understand and quantify these exchanges.

$$S_{l,j} = \alpha_j u_{x,j} Q_{l,j} \qquad \text{with } j = 1, 2 \text{ corresponding to the inlet and the outlet} \tag{5.1}$$

$$u_{x,j} = \underline{u_{l,j}} \cdot \underline{e_{x,j}} \tag{5.2}$$

5.4 Rectangular cross-section

Also described in the previous chapter, the assumption regarding the shape of the channels, namely the inlet and outlet, does not accurately represent the real geometry of PKWs. The space beneath the upstream overhangs is utilized by the flow in the inlet section (Figure 2.18), and the space beneath the downstream overhangs is utilized by the flow in the outlet section. Although some initial considerations were made regarding the improvement of the code in response to this issue, this avenue was temporarily abandoned but could be explored in future research. Indeed, the approach conditions for the flow in the inlet section could play a significant role, both in terms of the pressure drop and the reduction in effective width due to flow contraction. Since the inlet section serves as the "engine" of the PKW, investigating the impact of such an assumption on the discharge capacity would seem, "a priori", relevant and worthwhile.

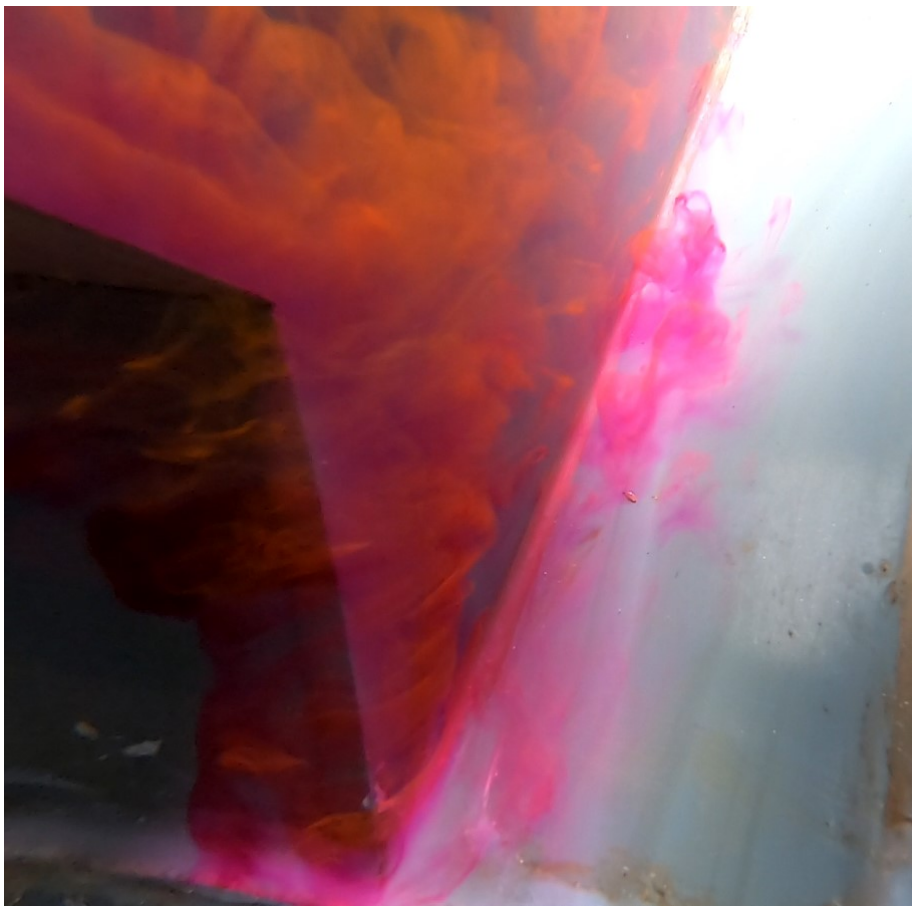

Figure 2.18: Uliège laboratory : inlet flow beneath the upstream overhangs - underwater camera

Figure 2.19 also illustrates that this space beneath the overhangs generates, at the inlet location, a recirculation linked to the flow contraction, resulting in head losses. In fact, the approach of modeling PKWs based on head loss in the inlet has been the subject of a study.

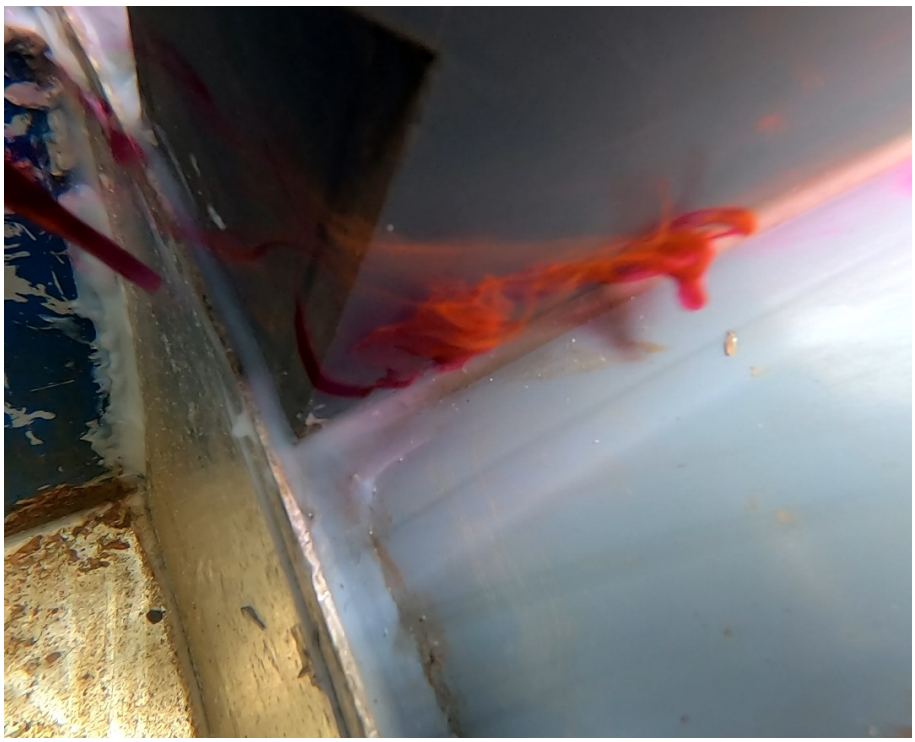

Figure 2.19: Uliège laboratory : head losses due to the upstream overhangs - underwater camera

5.5 List of the weaknesses and potential refinements

- ASSUMPTION 1 : 1D modeling ;
- ASSUMPTION 2 : No inclination of the main flow axis in the inlet;
- ASSUMPTION 3A : Lateral discharge coefficient $C_{D,Lat} = 0.385$ or 0.42 depending on crest profiling;
- ASSUMPTION 3B : Lateral terms are extracted from and injected in the volumes at the abscissa of the free surfaces that allows the computations of the lateral discharge, even if it was not those volumes that generates those free surfaces;
- ASSUMPTION 3C : no projection of the lateral flow along the x-axis is considered;
- ASSUMPTION 3D : $\alpha_{inlet} = \alpha_{outlet} = 1$, the lateral mass leaves and joins the flows with the same momentum/mass than the mass present in those flows;
- ASSUMPTION 4 : the spaces beneath the overhangs are neglected.

5.6 Accuracy of the initial model

The very first analysis of this study involved testing the old version of the code on the new dataset. Each configuration was then simulated for each of the laboratory-tested inflow rates.

The only freedom taken compared to the old model concerns the choice of numerical parameters. To optimize computation time, a convergence analysis was conducted, resulting in the following choices:

- Spatial step size of 1 cm;
- Maximum iteration count: 50,000;
- Tolerance for stabilizing the upstream water level: 1e-10.

Another degree of freedom, which will be discussed in greater detail in the subsequent sections of this work, is the selection of the lateral discharge coefficient. The previous version of the numerical model had been developed using an experimental dataset from the University of Liège laboratory, consisting solely of thick, non-profiled lateral crests. Given that the new dataset encompasses geometries from EPFL and EDF, featuring profiled crests, the choice of the lateral discharge coefficient, $C_{d,w,Lat}$, was theoretically set at 0.385 for University of Liège models and 0.42 for EPFL and EDF models. This choice could potentially influence the ensuing observations.

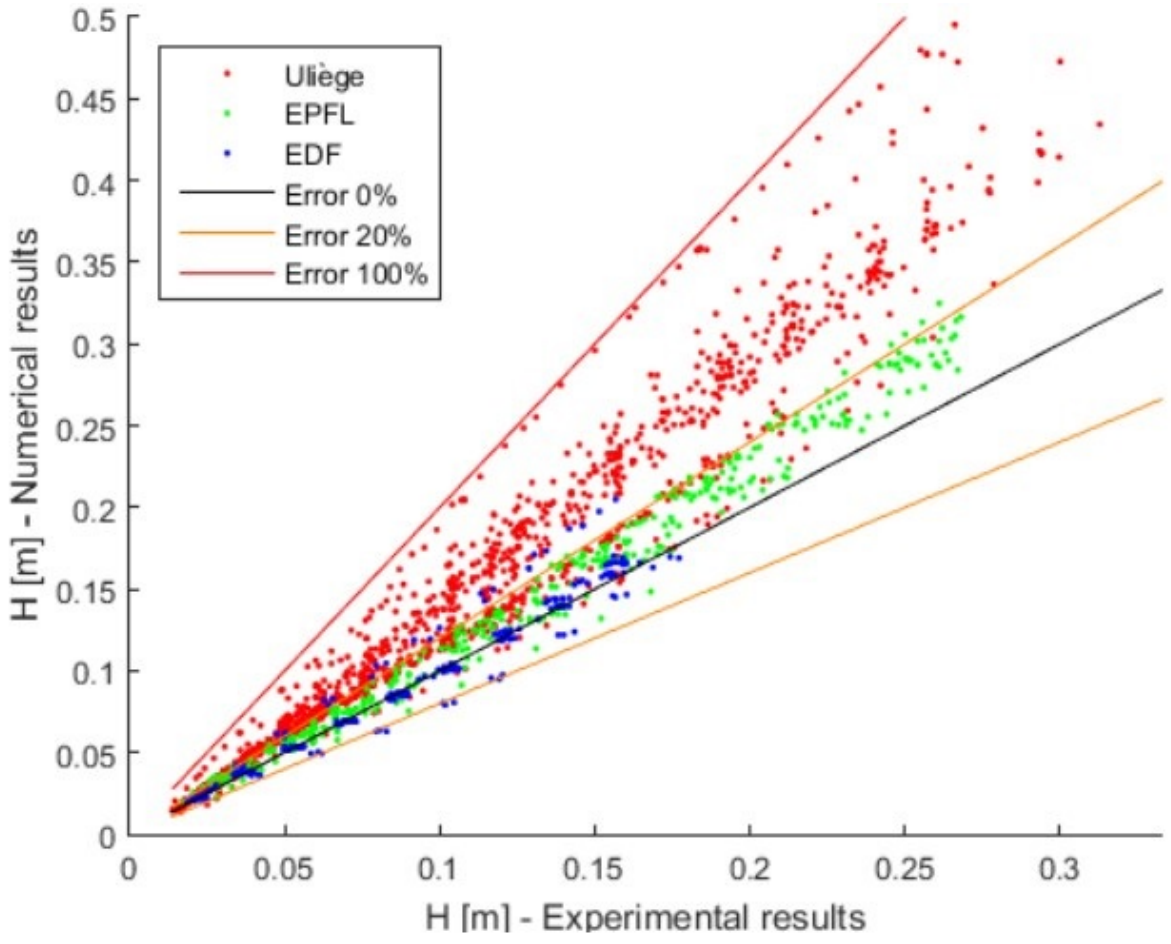

Figure 2.20: Accuracy of the initial model Wolf1DPKW - Comparison of the upstream head with physical model

Hence, Figure 2.20 illustrates the model's capacity to reproduce the experimental results. An intriguing initial observation concerns the model's almost systematic overestimation of the water level.

A secondary observation lies in the distinction among different laboratories. For University of Liège models, this overestimation is more pronounced, occasionally reaching an error of +100%. In the case of EPFL and EDF models, the tendency towards overestimation is less marked, with errors generally ranging between -20% and +20%.

This initial finding raises questions and prompts a reconsideration of the differentiation in the lateral discharge coefficient among models. As an initial intuition, the numerical observation that lateral exchanges predominantly occur from inlets to outlets suggests that increasing this coefficient enhances lateral discharge, resulting in elevated discharge rates and reduced upstream water levels. This intuition supports the possibility of improving the code by more appropriately selecting this modeling parameter. This notion will be further explored in the chapter dedicated to lateral exchanges.

These results can also be presented in the form of discharge-head curves, or more precisely, dimensionless upstream head - discharge coefficient curves. Accordingly, Figure 2.21 demonstrates that despite occasionally substantial model errors, the overall trend of each of these curves aligns with the characteristics described in previous studies [28][36][37].

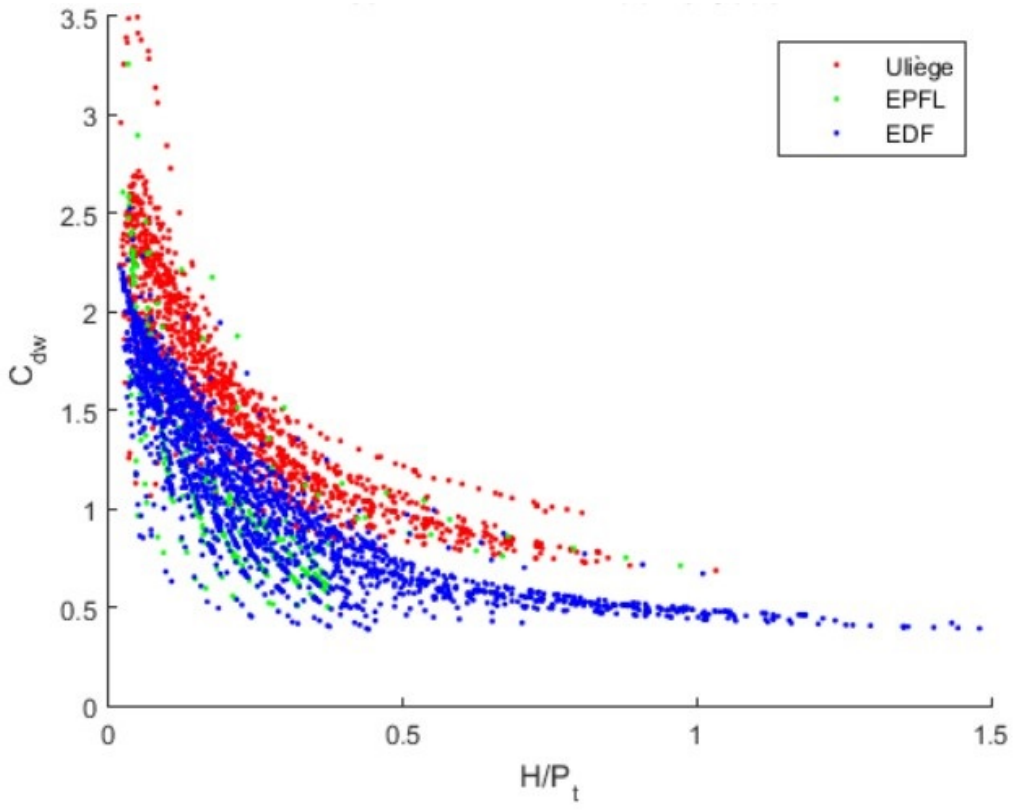

Figure 2.21: Non-dimensional head-discharge curves

In order to provide more quantitative estimations of this error – which will be valuable for assessing the extent of the model's potential improvement by the end of this work – a few statistics are worth noting.

- The mean error across the entire dataset is +24.1% (1971 measurements);
- The mean error for the University of Liège dataset is +31.8% (1360 measurements);
- The mean error for the EPFL dataset is +10.7% (380 measurements);
- The mean error for the EDF dataset is +1.84% (231 measurements).

Another observation pertains to the apparent error dependency on the imposed upstream discharge. As the upstream discharge increases (also resulting in an elevation of the upstream water head), the overestimation by the numerical model becomes more significant.

Once again, this is supported by a few quantitative data points. Classification is performed by grouping values of the dimensionless upstream water head, H/P_t :

- For $H/P_t \in [0.0, 0.2]$, the mean error is +17% (992 measurements);
- For $H/P_t \in [0.2, 0.4]$, the mean error is +26% (673 measurements);
- For $H/P_t \in [0.4, 0.6]$, the mean error is +43% (188 measurements);
- For $H/P_t > 0.8$, the mean error is +47% (107 measurements).

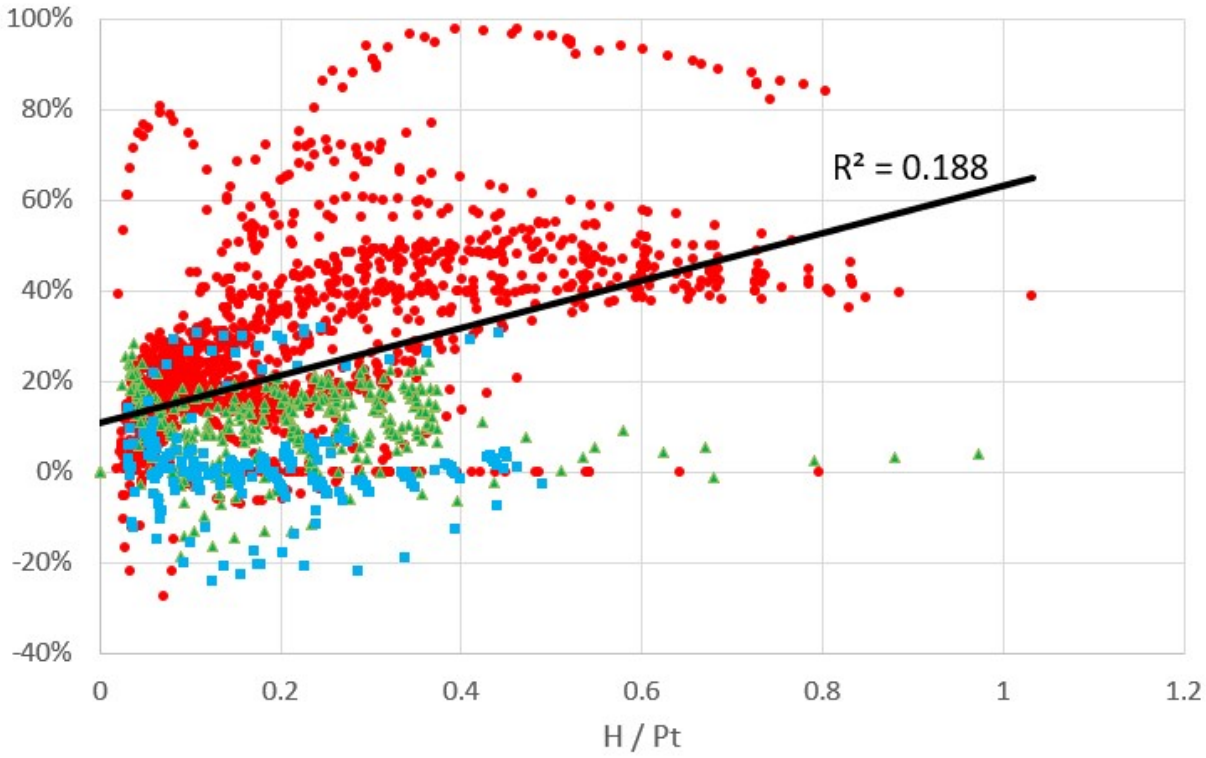

Figure 2.22: Discharge coefficient

Choosing to make the water head dimensionless by dividing it by P_t, the difference in altitude between the upstream PKW bed and its crest, could hold an implications. In the literature, it's not uncommon to normalize the upstream head by the height, without considering the water depth below the inlet openings [1]. In our case, the aim is simply to have a variable that is easily comparable across various geometries, and the choice is somewhat arbitrary. However, it enables a comparison of the obtained curves with standard weirs, often expressed in this manner.

5.7 Robustness of the initial model

A seldom-discussed dimension in this kind of research, but one that merits acknowledgment here, is the model's robustness. Indeed, the original code did not manage to converge on all configurations at all flow rates within the laboratory dataset.

Two factors are at play here:

- 13 cases are due to the format of input for geometric parameters. The code requires a singular value for each geometric dimension, while the provided model values exist within ranges. Consequently, this configuration is never represented in the trials. Nonetheless, it represents only one geometry out of the 113 available.
- 71 simulations do not converge, across different geometry types but typically at higher upstream flow rates. Upon analyzing these specific cases, it became evident that the con-

vergence criterion is a somewhat makeshift method that fails to capture all convergence possibilities or uses an overly restrictive tolerance criterion.

These 84 cases among nearly 2000 do not constitute a significant proportion of the results. Nevertheless, the issue deserves highlighting for three reasons:

- The increasing complexity of the model is leading to a rise in this proportion. Interpreting results becomes less straightforward when a small number of simulations is studied, as in a sensitivity analysis of specific parameters.

User satisfaction substantially decreases if a portion of their simulations fails to converge without an alternative solution. Notably, for the preliminary design of a real-world structure, attention is focused on a limited number of results, each of which may hold significance.

Consequently, a chapter is dedicated to this aspect. Since this analysis was not deemed a priority within the scope of this study, simulations that did not converge could not be re-run after improvements and integrated into the figures of this report. Hence, the absence of certain data points in the remainder of this work is not an uncommon occurrence.

6 Objectives of this thesis

Semi-empirical formulas provide an initial estimation of the hydraulic performance of Piano Key Weirs (PKWs). While useful in the pre-design phase, this approach has its limitations. The empirical coefficients derived from formula calibration strongly depend on a specific database. This semi-empirical approach also falls short in identifying the physical phenomena that will occur on the PKW, such as the control section position and outlet submergence.

On the other hand, physical models are particularly suitable for observing the hydraulic behavior of a structure. However, the costs and time required for physical model studies often limit them to the final design phase, where they are used to validate the selected dimensions and calculated hydraulic performance. This approach is less suitable for a parametric analysis involving a large number of geometric parameters across a wide range of values.

By solving the equations of fluid mechanics, numerical models are inherently based on physics rather than empirical data. The assumptions in numerical models vary depending on their nature (1D, 2D, or 3D) and spatial meshing choices. 3D models generally require more development time due to meshing considerations and involve longer simulation times. 2D and 1D models are not always appropriate as they assume a strong hypothesis of uniformly distributed velocities in the integrated dimension, with velocities primarily oriented in two or one

direction. 3D numerical models, therefore, resemble physical models more closely. They are positioned slightly earlier in the design phase and can be validated against physical models to simulate a wider range of flow rates, approach conditions, and initial system states.

Coarser meshes or 1D and 2D approaches generally enable faster and less costly simulations, allowing for a broader parametric analysis. Thus, they bridge the gap between empirical and semi-empirical approaches on one hand, and complex 3D mesh models and physical models on the other hand.

The objective of this master's thesis is to improve a 1D numerical model. As described above, the aim of such a model is to simulate a large number of geometries quickly and cost-effectively, while maintaining a physically-based approach. The idea is to limit restrictive assumptions in order to preserve the validity of the model over the widest possible range of geometries. The limitations of the model will be discussed, and the chosen assumptions will be justified. A 1D model for PKW modeling already exists, and the objective is to improve upon it, creating a fast, transparent, and intuitive numerical simulation tool that can be validated against a diverse database.

Although the overall functioning of the code has not been detailed yet, for those familiar with the subject, the objective is to intelligently implement the inclination of the flow axis in the PKW's inlet.

Chapter 3

Constructing a statistically representative dataset

1 A deeper analysis of the database weaknesses

As mentioned earlier, the database, which is not always statistically representative, poses a limitation to fully exploit the results of simulations on both the new and old code versions.

As previously described, some laboratories have provided more models than others, with common characteristics across many of their geometries, such as lateral crest profiles. Additionally, some laboratories have densely covered a wider range of upstream flow rates:

- ULiège has 1360 measurements for 40 configurations, averaging 38 measurements per configuration.
- EPFL has 380 measurements for 49 configurations, averaging 8 measurements per configuration.
- EDF has 231 measurements for 24 configurations, averaging 10 measurements per configuration.

Furthermore, considering the sensitivity analyses to be conducted, a more in-depth analysis of the dataset revealed that certain ranges of geometric parameters are more extensively represented than others.

One evident reason is the concentration of tests within the ranges deemed by the literature to be close to the techno-economic optimum. For instance, configurations with a length-to-width ratio (L/W) close to or equal to 3 are predominantly featured (L/W = 3 for 88 out of 113 configurations).

Another rationale can be understood by examining prior research work. A significant number of configurations were constructed with the aim of studying a single geometric parameter. This results in a high density of configurations across all other dimensions. For instance, configurations 41, 42, and 43 from EPFL focused on investigating the impact of parapets on the frontal crests of the inlets or outlets. As these parapets do not affect any of the non-dimensional parameters used to classify PKWs, these three configurations are indistinguishable from the sensitivity analyses conducted in this study.

To mitigate the disproportionate overrepresentation of certain parameter ranges in the interpretation of results and model calibration, subsampling was performed. This process facilitates both a more robust calibration for non-standard geometries and easier qualitative analysis, all while retaining relevance.

However, reducing the dataset to this subsample somewhat deprives us of a substantial amount of hard-to-collect data.

Furthermore, retaining the entirety of the data despite this bias can still hold value. As researchers' understanding of these structures grows, they tend to focus on parameters they fix to standards that progressively approach a techno-economic optimum. Consequently, the relative importance of these models becomes higher in calibration, to the detriment of less standard models, which could prove beneficial.

2 Harmonizing the number of tested discharges per configuration

Reducing and standardizing the number of upstream discharges to be simulated for each configuration offers a dual advantage: it decreases computation time while enhancing the statistical representativeness of the results.

To achieve this, several decisions need to be made.

The first decision concerns the number of discharges per configuration. This choice aligns with a broader optimization goal of computation time. After a quick estimation of the number of parameters to simulate for the initial sensitivity analyses, the decision was made to employ five discharges per geometry.

The second decision revolves around the range of discharges to consider and how to discretize this range. The latter point was quickly resolved with a straightforward discretization at a constant discharge interval. However, determining the appropriate range of discharges

proved to be more intricate.

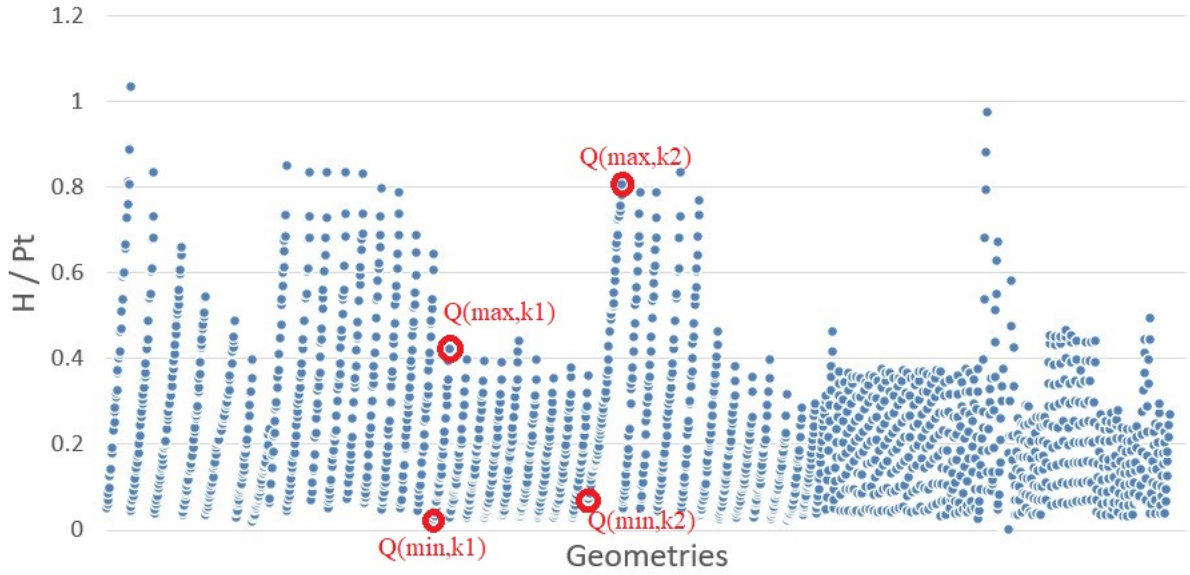

Figure 3.1: Range and density of tested discharges for all configurations

On one hand, it was possible to align with researchers' intuitions about their models by preserving the usage ranges retained by each of them, even if these choices differed from one another (as illustrated in Figure 3.1). Numerically, this ensured that each numerically simulated discharge had its equivalent, or a close match, in laboratory measurements. This approach also retained a maximum amount of data by not excluding the highest discharges that might not have counterparts for all configurations.

On the other hand, another possibility was to select discharges for simulation in a way that maintained the same values of dimensionless heads between each geometry. The advantage of this second option is a higher level of relevance in the comparison between configurations, achieved by harmonizing the discharge ranges for each geometry (refer to Figure 3.1). However, the range of covered discharges would have been constrained by the geometry with the most limited range. Moreover, the model takes an upstream discharge as input to provide a head as output. Based on laboratory tests, the empirical head-discharge relationships could have provided estimates of discharges through reverse engineering.

However, the focus here is on targeting dimensionless heads. Yet, as briefly mentioned earlier, the choice of dimensionless variable for head adimensionalization has a direct impact on the discharges retained. Indeed, studies have shown that the flow physics over PKWs are influenced by both the dimensionless variables H/P_i and H/P_t [1]. While the question of adimensionalizing was not relevant for thick weirs, sharp-crested weirs, or ogee-crested weirs due to their nature, PKWs present a wider range of geometric possibilities that significantly affect flow dynamics. As the variables P_i and P_t are scarcely correlated (see Figure 3.2), there seems to be no a priori more pertinent choice to optimize comparison.

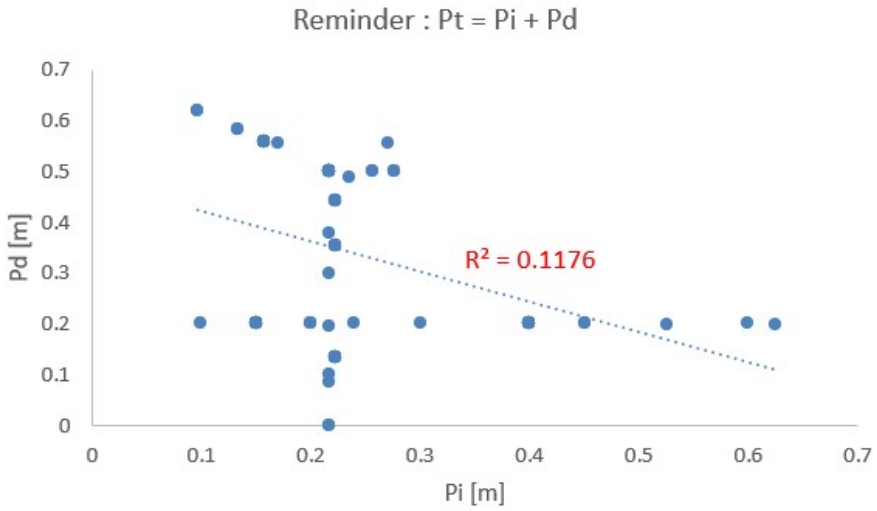

Figure 3.2: Weak correlation between the variables P_i and P_t.

Thus, even though the second approach is appealing for geometry comparison, it has been disregarded.

3 Selection of emphasized non-dimensional parameters

Previous studies on PKW identified five influential dimensionless ratios for the hydraulic performance of PKWs:

- Crest length L/W [38][39][40][41];
- Weir height P/W_u[1][38][41];
- Keys width W_i/W_o[1][38][41][42][43][44];
- Overhangs length B_o/B_i[1][41].

While flow rate constitutes the primary influencing parameter, the addition of these four geometric parameters further shapes the hydraulic behavior. Subsequently, improvements in the code will lead to sensitivity analyses on modeling variables. However, attempting to explore each of these variables comprehensively with a sufficiently high density of data points for conclusive insights would result in computationally intensive tasks and intricate result analyses.

As a consequence, a solid grasp of the underlying physics is essential in order to select geometric parameters that are likely to yield meaningful results, forming the basis for constructing a meaningful subset of configurations.

4 Crest length L/W

The crest length is a primary advantage of Piano Key Weirs (PKWs). By providing an extended crest length that enables the controlled discharge from upstream to downstream, PKWs optimize their efficiency at low heads. At higher heads, the discharge coefficient diminishes and this competitive edge gradually fades, with lateral discharge becoming relatively less significant compared to frontal discharges.

On one hand, this parameter has already been extensively addressed in existing literature. On the other hand, the feasibility of conducting a parametric study exclusively on this specific ratio is hindered by the nature of the database. As previously explained, the majority of configurations feature an exactly equal L/W ratio. Furthermore, as depicted in Figure 3.3, the scope for varying this ratio is relatively constrained.

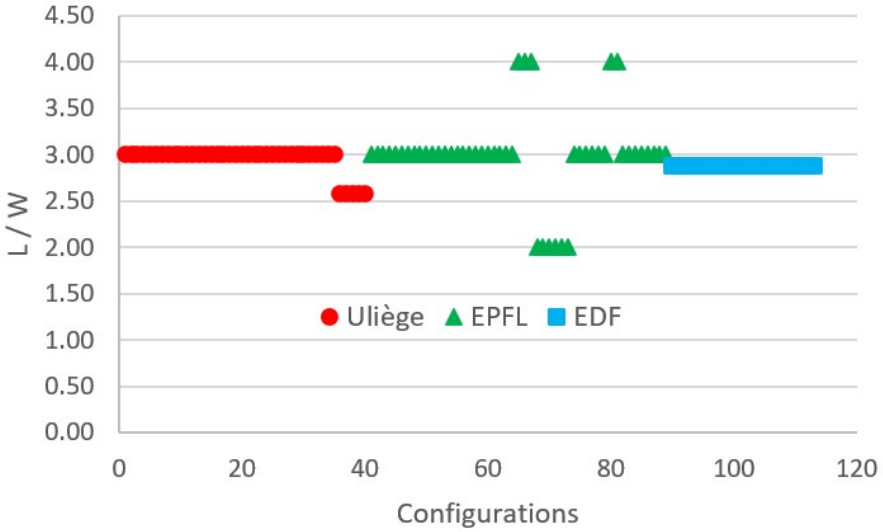

Figure 3.3: Distribution of the L/W ratio in the database configurations

Primarily due to the former argument, although this parameter holds substantial influence over PKW discharge capacity, it is not included among the parameters investigated in this study.

5 Weir height P/W_u or bottom slope in the inlet $\theta_{b,i}$?

"On the 1:10 scale model, the flow contraction at the inlet key entrance and the apparition of a control section in the downstream part of the key have been identified as the two main reasons of the observed efficiency decrease with increasing heads. As the increase of the weir height decreases the flow velocities along the inlet key, it must increase significantly the PKW efficiency." [1]

The influence of this parameter on the PKW discharge is indeed confirmed. However, what particularly captures our attention in this study is the impact of geometry on the accuracy of the water level approach (1D) modeling. Among the model's weaknesses and areas for improvement, one aspect is the inclination of the flow axis in the inlet. One avenue of consideration is that the optimal inclination for modeling could be contingent upon the bottom slope in the inlet.

As depicted in Figure 3.4, the configurations exhibit a wide range of relative heights within the interval [0.3, 0.9], and the Uliège configurations facilitate the exploration of flow behavior up to a ratio of 2. Past research also suggests that this expanded range might encompass the economic optimum [1].

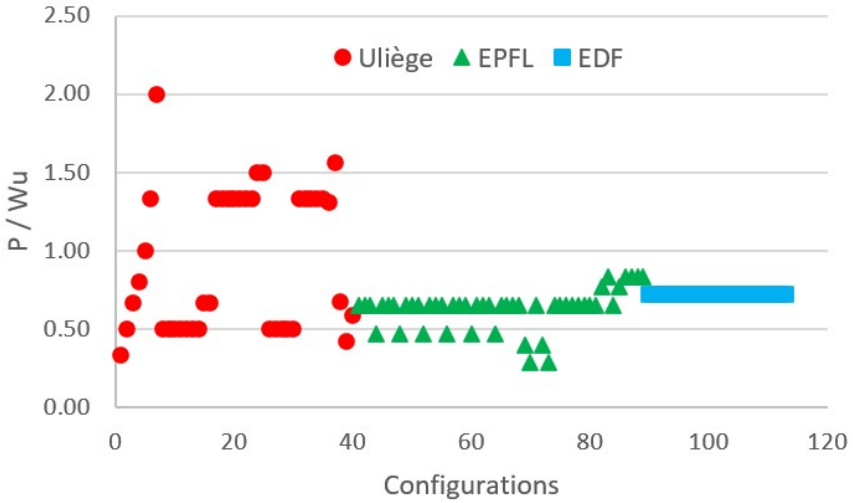

Figure 3.4: Distribution of the P/W_u ratio in the database configurations

However, even though the relative height is a function of the bottom slope:

$$\theta_{b,i} = \text{atan}\left(\frac{P_i}{B - B_o}\right) = f(P_i) \tag{5.1}$$

This parameter also involves the unit PKW width. Indeed, Figure 3.5 depicts a similar trend, and Figure 3.6 quantifies the correlation between the two variables.

Although they are linked, the correlation is far from perfect, and certain deviations from the trend curve have motivated the decision to retain the bottom slope of the inlet as the influencing parameter, rather than the relative height.

A limitation that quickly becomes apparent in this approach is the model's weak ability to study the impact of a parapet on the frontal crest of the inlet. This parapet will deflect the flow into the inlet, resulting in an effect somewhat analogous to a steeper bottom slope. However, the parapet has no influence on the bottom slope parameter but does impact the relative height.

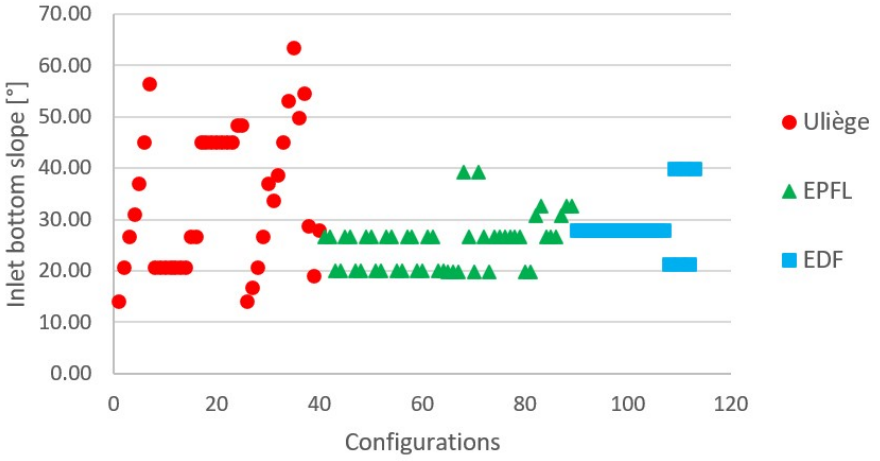

Figure 3.5: Distribution of the inlet bottom slope ($\theta_{b,i}$) in the database configurations

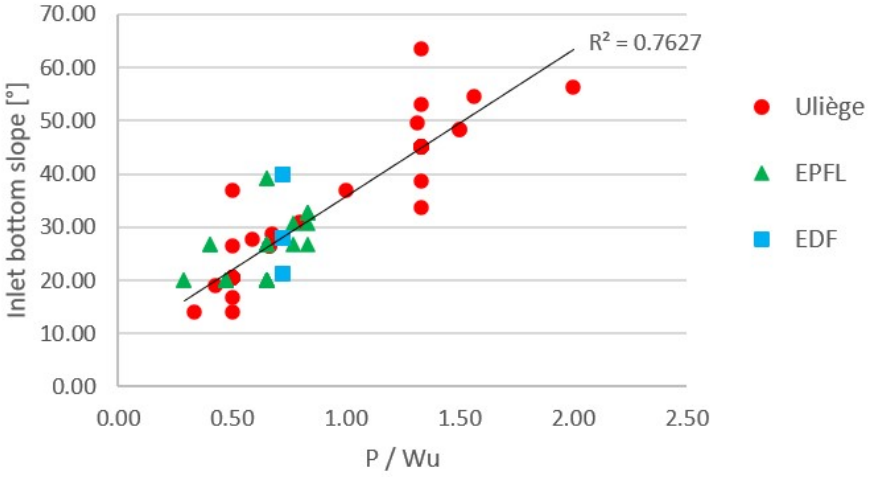

Figure 3.6: Correlation between relative height and inlet bottom slope

Given the significance of this parameter on the first aspect of improvement and while keeping in mind the overall computational time for the simulations, the choice was made to categorize the bottom slope into five classes, ranging from the lowest (Class A: 14 degrees) to the steepest (Class E: 56 degrees) within the database.

Furthermore, due to the model's limitations concerning parapets, a configuration with a inlet parapets will be retained in the subsampling to try to identify any atypical behavior for this type of geometry.

6 Keys width W_i/W_o

The width ratio of the PKW W_i/W_o also plays a significant role in the weir's discharge capacity. An outlet that is relatively too narrow will become submerged more quickly, resulting in higher water levels in the outlet. This situation negatively impacts lateral flow and the upstream water level of the weir.

Similar to the relative height parameter, our focus is primarily on understanding the influence of this parameter on flow characteristics, rather than solely seeking the techno-economic optimum. Inaccurate modeling of lateral exchanges could manifest differently in the model's accuracy based on this parameter.

Previous analyses *[...] conclude to an optimal W_i/W_o ratio close to 1.25. However, variations of this ratio between 1 and 1.5 don't change significantly the discharge capacity of the PKW. For a PKW design based on pure hydraulic, a ratio of 1.25 is optimal. According to techno-economic interests, a symmetric configuration seems more relevant as it enables the use of precast elements.* [1]. Therefore, this parameter is included in constructing the sample, but with only three categories:

- Class 1: $W_i/W_o < 1$;
- Class 2: $W_i/W_o \in [1, 1.5]$;
- Class 3: $W_i/W_o > 1.5$.

Figure 3.7 also illustrates the diversity of the database in terms of width ratios. It includes ratios ranging from 0.5 to over 2.

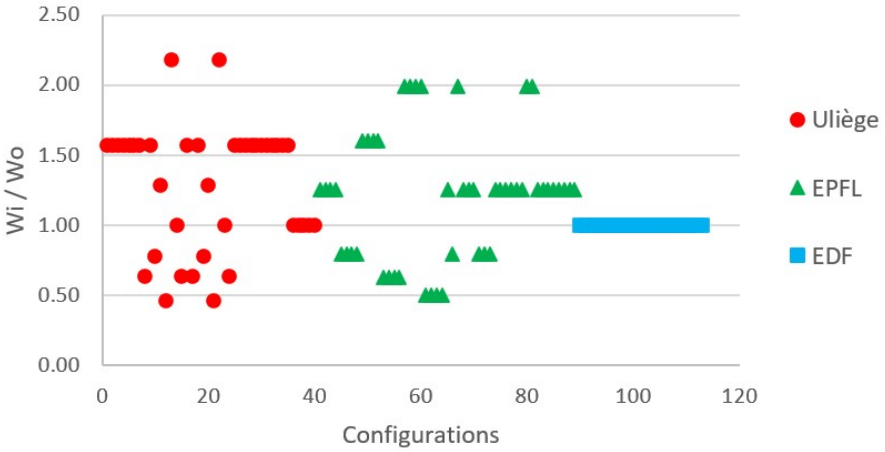

Figure 3.7: Distribution of the W_i/W_o ratio in the database configurations

7 Overhangs length B_o/B_i

One avenue of improvement concerns the consideration of the space beneath the overhangs. In this context, it might have been evident that the ratio of upstream and downstream overhang

lengths B_o/B_i would be a parameter of primary importance.

However, the database provides only limited variation for this parameter, making any sensitivity analysis or modeling calibration more challenging (see Figure 3.8).

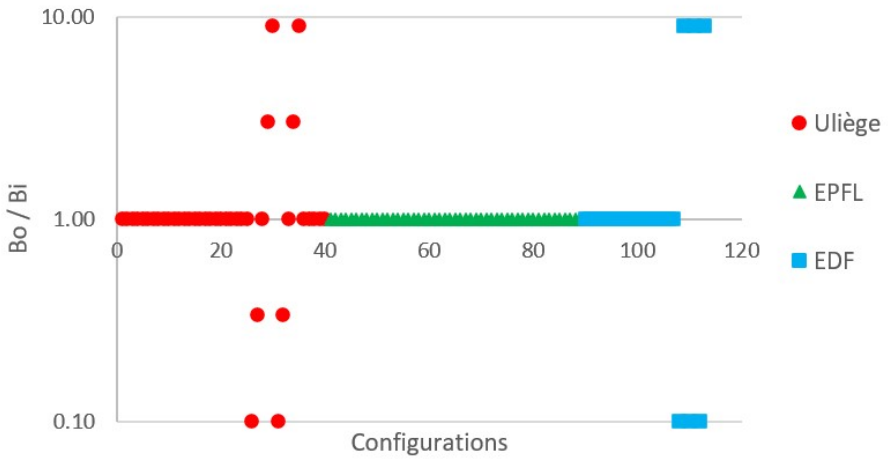

Figure 3.8: Distribution of the B_o/B_i ratio in the database configurations

Furthermore, partly due to this lack of variation, this avenue of improvement was not pursued. Additionally, the relationship between flow dynamics and this ratio does not appear to be the same depending on other geometric parameters. Creating a representative subset would have required properly mapping these three variables to cover most potential cases.

Consequently, this parameter is not included in the sampling. However, in order to detect any atypical behavior that might be applicable across all these configurations, a single Type B PKW is included.

8 Summary of the final sample

n the preceding sections, certain choices have emerged for constructing the subsampling of simulations to be performed:

- Five flow rates per configuration, encompassing the minimum and maximum laboratory-tested flow rates for these configurations;
- Five classes of inlet bed slope configurations $\theta_{i,b}$ (A to E);
- One configuration with parapets at the inlet;
- Three classes of width ratio W_i/W_o (1 to 3);

- One configuration of type B (without upstream overhangs).

To accurately map the two variables giving rise to classification, this totals to $3 * 5 + 2$ configurations, each with 5 flow rates. However, the database contains no configurations with extreme bed slope (A and E) and a low width ratio (1 and 2). This brings the total to 13 configurations out of the 113 present in the database. With five flow rates each, this results in a total of 65 simulations for a fixed set of modeling variables.

As shown in Figure 3.9, several choices are available for most categories of configurations to represent. The choice is somewhat arbitrary. However, one of the objectives has been to preserve, as far as possible, perfectly identical ratios within a class.

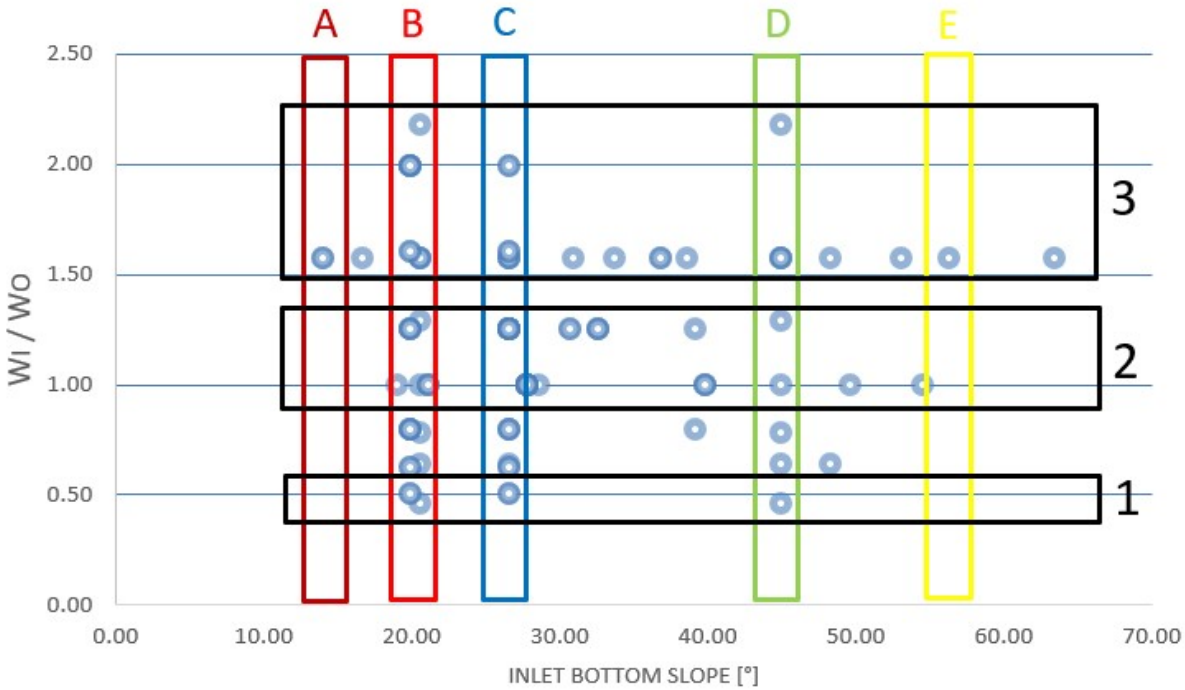

Figure 3.9: Mapping of configurations based on W_i/W_o and $\theta_{i,b}$ parameters

Tables 3.1 and 3.2 summarize the geometric characteristics of the performed sampling.

Table 3.1: New sample of configurations - Part 1

Classification	Config ID	ID first	ID last	Lab	Config Name	Crest type	P_o	P_i	R_o	R_i	P_d	W	Nb Units
(-)	(-)	(-)	(-)	(-)	(-)	(-)	(m)	(m)	(m)	(m)	(m)	(m)	(-)
A3	1	1	45	ULg	Model 2 - 1	Broad	0.1	0.1	0	0	0.203	0.75	2.5
B1	64	1540	1546	EPFL	24	Round	0.157	0.157	0	0	0.56	0.5	1.5
B2	14	511	544	ULg	Model 3 - 14	Broad	0.15	0.15	0	0	0.203	0.75	2.5
B3	51	1439	1446	EPFL	11	Round	0.217	0.157	0	0	0.56	0.5	1.5
C1	61	1516	1523	EPFL	21	Round	0.217	0.217	0	0	0.5	0.5	1.5
C2	77	1641	1652	EPFL	37	Round	0.217	0.217	0	0	0.1	0.5	1.5
C3	58	1493	1500	EPFL	18	Round	0.157	0.217	0	0	0.5	0.5	1.5
D1	21	734	765	ULg	Model 3 - 21	Broad	0.4	0.4	0	0	0.203	0.75	2.5
D2	20	701	733	ULg	Model 3 - 20	Broad	0.4	0.4	0	0	0.203	0.75	2.5
D3	22	766	798	ULg	Model 3 - 22	Broad	0.4	0.4	0	0	0.203	0.75	2.5
E3	7	272	302	ULg	Model 2 - 7	Broad	0.6	0.6	0	0	0.203	0.75	2.5
B'	63	1532	1539	EPFL	23	Round	0.217	0.157	0	0	0.56	0.5	1.5
B''	110	1936	1944	EDF	B2-P1	Broad	0.222	0.222	0	0	0.355	1.99	6.5

Table 3.2: New sample of configurations - Part 2

Classification	W_u	W_o	W_i	T_s	B	B_o	B_i	Qmin	Qmax	Teta_i	L/W	W_i/W_o	B_o/B_i
(-)	(m)	(m)	(m)	(m)	(m)	(m)	(m)	(m^2/s)	(m^2/s)	(°)			
A3	0.3	0.105	0.165	0.015	0.6	0.2	0.2	0.014	0.532	14.0	3.00	1.57	1.00
B1	0.333	0.195	0.098	0.02	0.667	0.233	0.233	0.054	0.352	19.9	3.00	0.50	1.00
B2	0.3	0.135	0.135	0.015	0.6	0.2	0.2	0.016	0.514	20.6	3.00	1.00	1.00
B3	0.333	0.113	0.181	0.02	0.667	0.233	0.233	0.05	0.372	19.9	3.00	1.60	1.00
C1	0.333	0.195	0.098	0.02	0.667	0.233	0.233	0.046	0.4	26.6	3.00	0.50	1.00
C2	0.333	0.13	0.163	0.02	0.667	0.233	0.233	0.03	0.329	26.6	3.00	1.25	1.00
C3	0.333	0.098	0.195	0.02	0.667	0.233	0.233	0.047	0.372	26.6	3.00	1.99	1.00
D1	0.3	0.185	0.085	0.015	0.6	0.2	0.2	0.025	0.548	45.0	3.00	0.46	1.00
D2	0.3	0.118	0.152	0.015	0.6	0.2	0.2	0.019	0.549	45.0	3.00	1.29	1.00
D3	0.3	0.085	0.185	0.015	0.6	0.2	0.2	0.019	0.547	45.0	3.00	2.18	1.00
E3	0.3	0.105	0.165	0.015	0.6	0.2	0.2	0.018	0.454	56.3	3.00	1.57	1.00
B'	0.333	0.195	0.098	0.02	0.667	0.233	0.233	0.053	0.373	19.9	3.00	0.50	1.00
B''	0.306	0.133	0.133	0.02	0.573	0	0.307	0.025	0.216	21.2	2.87	1.00	0.00

Chapter 4

Results & Discussion

1 Inclination of the flow axis within the inlet

1.1 Physical and experimental rationale

The first improvement to the model concerns the inclination of the flow axis within the inlet. Laboratory observations reveal that streamline patterns within the inlet tend to incline, particularly in the lower section of the inlet and for configurations where the bed slope is substantial (see figure 4.1).

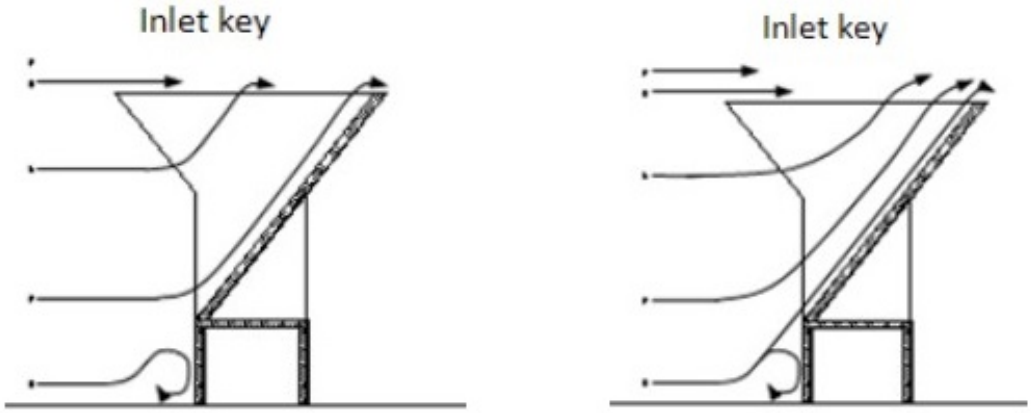

Figure 4.1: *Streamlines for (left) low heads and (right) high heads* [1]

Assuming a horizontal flow axis, both vertical and lateral components of velocity are neglected for pressure distribution (hydrostatic, perpendicular to the flow, i.e., vertically). As a reminder, regarding mass and momentum exchanges, lateral exchange modeling partially addresses the issue of lateral velocity components. However, no consideration is given to the vertical velocity component.

By inclining the flow axis relative to the horizontal plane, the hypothesis of a hydrostatic pressure distribution is maintained, albeit along an inclined axis. This approach partially accounts for the vertical velocity component, at the expense of a portion of the horizontal com-

ponent.

Real-world flow is more complex than unilateral flow along a horizontal or inclined axis, as streamlines are not parallel. In tilting the flow axis, the aim is not to perfectly model the inlet flow, but rather to mitigate error by seeking a flow axis that corresponds to the average inclination of velocities at a flow section.

Due to the absence of more specific measurements, numerical experiments are constrained to applying a constant inclination throughout the entire inclined section of the inlet, and this inclination remains constant for all flow rates. Based on the intuition that bottom streamlines tend to align with the bed slope, a proportional relationship between the bed slope and the flow axis inclination is assumed. Thus, the flow axis inclination within the inlet is parameterized in the code as a percentage of the bed slope of the considered geometry. Upstream, in the reservoir and adjacent to the outlet overhang, the assumption of horizontal flow is retained. Downstream of the downstream crest of the inlet, the assumption of a 45-degree bed slope with an axis parallel to this slope is maintained to ensure supercritical flow downstream of the structure.

1.2 Physically meaningful range of values

In order to maintain a physically-based approach, careful definition of the range of values to be numerically simulated is essential. An excessively wide range could lead to model calibration that inadequately represents the underlying physical phenomena, an outcome this work aims to avoid.

To establish meaningful bounds for the inclinations, an approach was adopted that relies on velocity profiles aligned with observations and an understanding of flow dynamics within the inlet.

For the maximum inclination, a uniform velocity profile across the cross-section perpendicular to the flow axis is assumed (see Figure 4.2). This assumption is based on the insight that the frictional bottom boundary in the inlet slows down the flow at the bottom, preventing the bottom flow from exceeding surface flow. Laboratory measurements also support this assumption (Figure 4.4, [1]). This profile is considered consistent across the entire width of the flow, aligning with the unidirectional flow assumption. The extreme case corresponds to a geometry with a steep incline in the inlet and a low discharge. In this scenario, the free surface is nearly horizontal, and the weighted average inclination over the section, considering velocities, results in a maximum slope of 50% of the bed slope.

For the minimum inclination, a logarithmic longitudinal velocity profile is chosen (see Figure

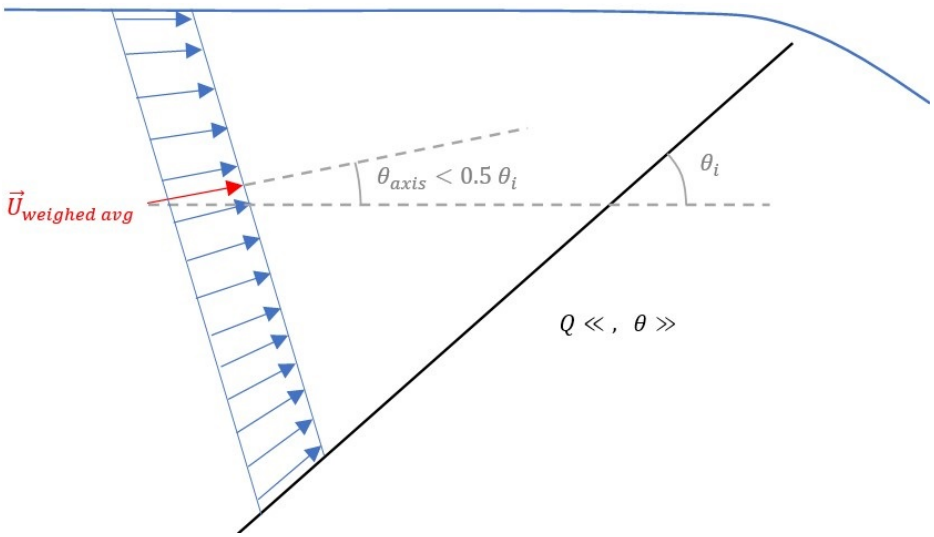

Figure 4.2: Schematic representation of velocity profile across a cross-Section: low discharge and steeply inclined inlet

4.3). The lower velocities at the bottom and higher velocities at the surface favor the weighting of flowlines with a shallower ascent. The extreme case occurs for a gently sloping inlet geometry crossed by a high discharge. Here, the free surface exhibits a pronounced reverse slope (downward slope in the flow direction). Thus, the weighted average of velocity vectors' inclinations could be near horizontal or even yield a resultant velocity slope in the downward direction. This finding, contrary to the initial concept behind this improvement approach, prompted a tentative decision to restrict inclinations to 0% and then to -10% of the bed slope during the initial testing phases.

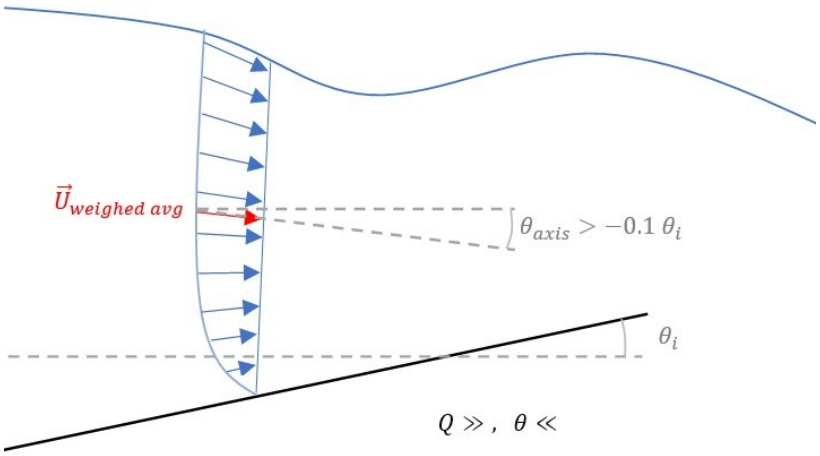

Figure 4.3: Schematic representation of velocity profile across a cross-Section: high discharge and mildly inclined inlet

It is important to emphasize that these assumptions regarding the longitudinal velocity profile within the inlet aim solely to set inclination bounds for the flow axis. Given the fully three-dimensional nature of the flow, with flowlines fed by under-overhang spaces upstream, flowlines exiting laterally from the inlet, and frictional lateral walls, these assumptions are hardly reliable for other applications. This explanation also highlights the potential for explor-

ing flow axis inclinations significantly less than -10% of the bed slope for certain geometries and high discharges.

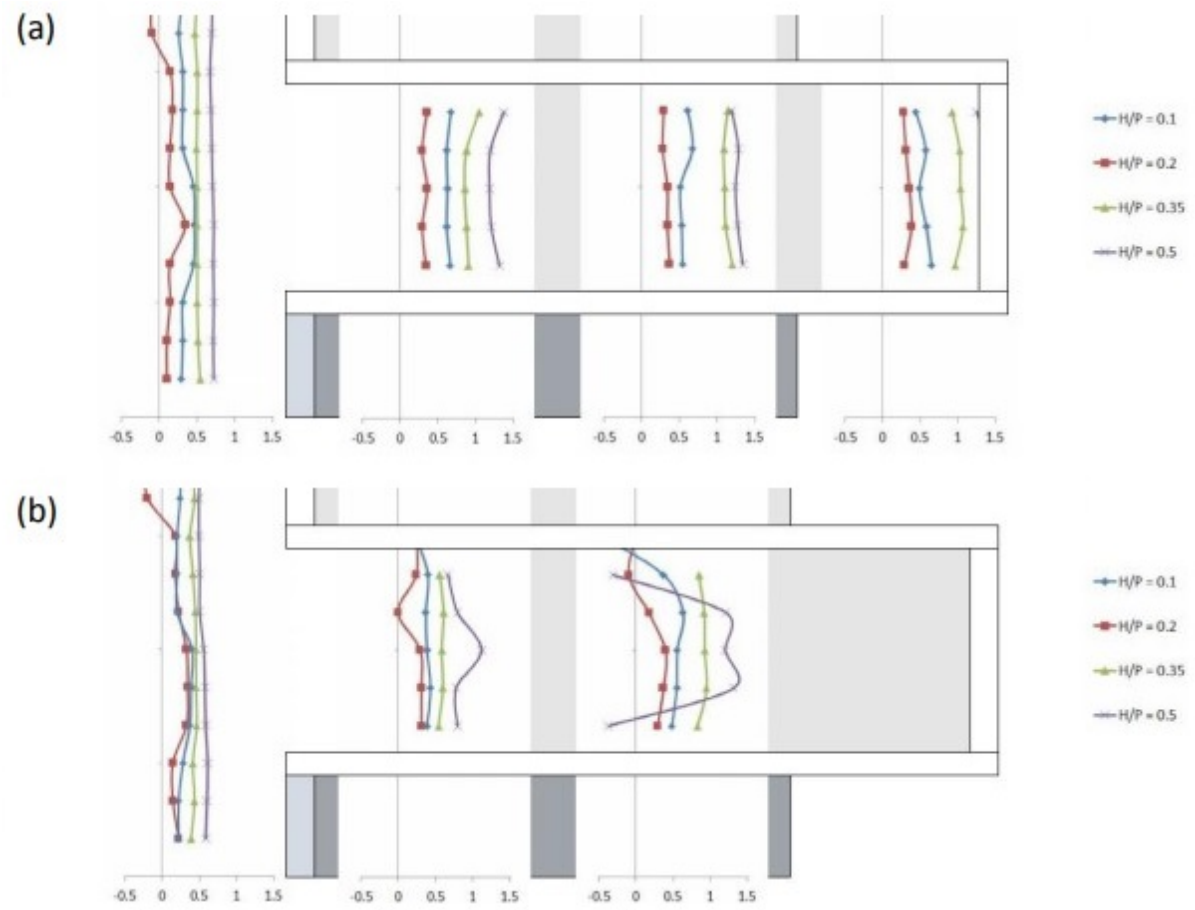

Figure 4.4: *Horizontal velocity profiles (m/s): (a) over the weir Z = 0.75 m; (b) in the weir Z = 0.55 m* [1]

1.3 Implementation

During the implementation phase, a numerical obstacle emerged. By inclining the flow axis within the inlet, with a varying inclination between the inclined sections and the upstream portion, the projected free surfaces of two distinct volumes could come into conflict. Specifically, when the flow axis is horizontal upstream, the free surfaces are projected vertically. However, in the inclined section within the inlet, the flow axis may be inclined upwards, projecting a free surface upstream of the horizontal abscissa of the final volume. This issue, which did not arise in the previous version of the code, required a solution to be devised.

Figure 4.5 illustrates this problem by depicting the free surfaces obtained during the first iteration of the enhanced code version, using initial conditions based on discharges and cross-sections variables derived from a stabilized water line of the previous code version.

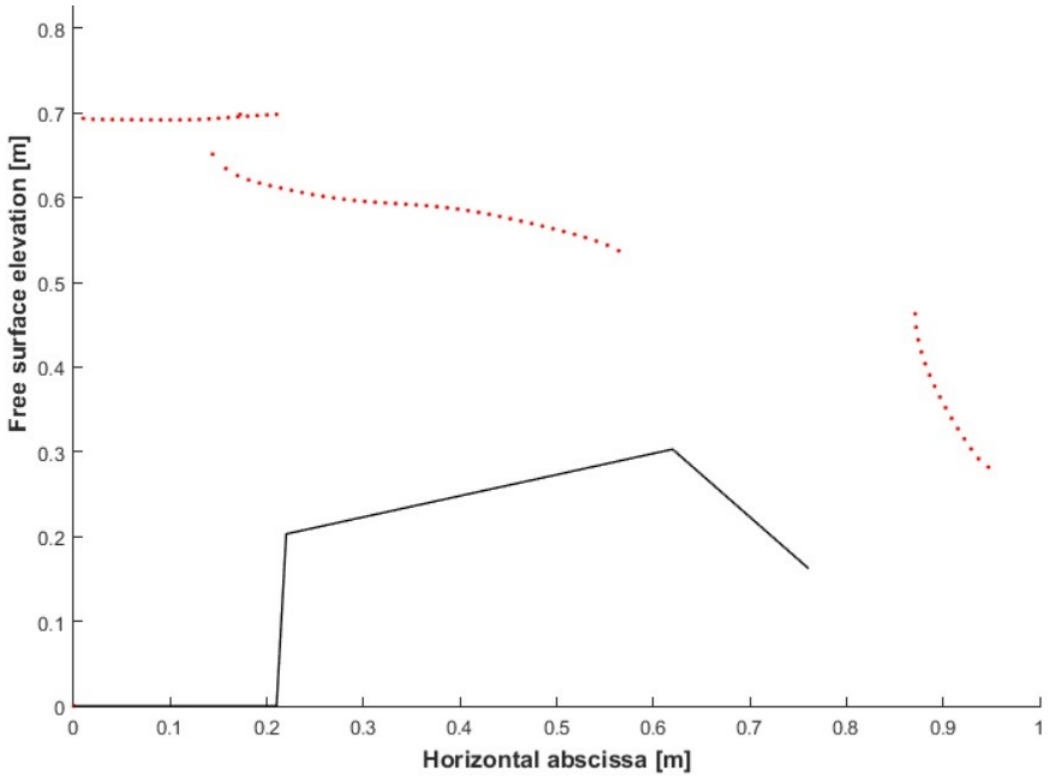

Figure 4.5: Conflictual free surfaces due to inlet inclination

As the free surfaces are consistently recalculated in a horizontal-vertical reference frame for lateral exchange calculations, a decision must be made regarding which free surface predominates in this conflict.

To study the consequences of this choice, three options were considered and tested on a standard configuration for various flow axis inclinations:

1. Prioritize information from upstream volumes;
2. Prioritize information from downstream volumes;
3. Compute an average between upstream and downstream information, utilizing a calculation system that accounts for non-constant deviations in horizontal abscissas of projected free surfaces from downstream information.

The results associated with these three options for this specific configuration highlight two key observations (Figure 4.6) :

- Inclining the flow axis upward within the inlet does not, for this particular configuration, lead to a reduction in upstream head. Given the consistent overestimation of head with the numerical model, this initial observation does not offer a very optimistic outlook regarding this improvement approach ;

- The results are quite comparable among all three options, with a slightly lower error observed for option 1. As a result, option 1 was selected as the preferred choice for the numerical model.

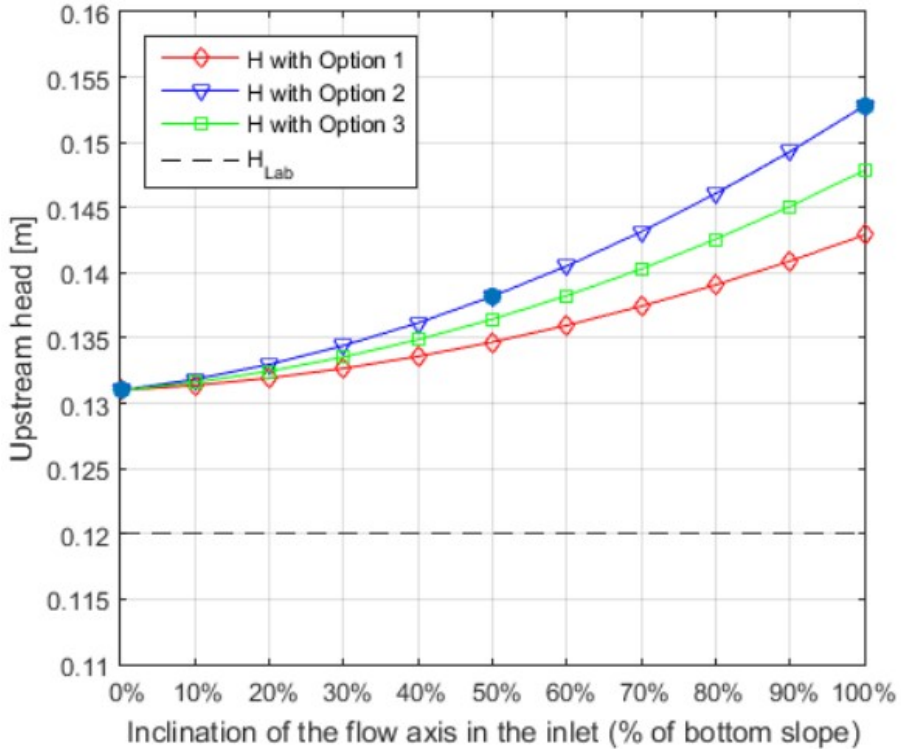

Figure 4.6: Comparative analysis of of various flow axis inclination options

1.4 Results - first range

The initial numerical experiments were conducted with the sole modification from the previous version of the code being the inclination of the flow axis within the inlet (θ). As a reminder, this inclination is expressed as a percentage of the bottom slope within the inlet, denoted as θ_i.

These initial experiments focus on the selection presented in Section 3. This approach serves to reduce computation times and facilitate a more straightforward analysis of the results. Since it has been established earlier that the upstream discharge affects the model's accuracy, the subsequent analyses were systematically carried out over five different levels of discharge, spanning the range of H/P from 0.02 to 0.3. When the upstream discharge does not significantly impact the conclusions, only graphs corresponding to the extreme discharges are presented to enhance clarity.

Hence, Figures 4.7 and 4.8 depict the results obtained at low and high discharge, respectively. The accuracy of the numerical model is assessed by comparing the numerically calculated upstream head (H_{Num}) with the laboratory-measured value (H_{Lab}). For a given upstream

discharge and specific configuration, the laboratory-measured headwater level (H_{Lab}) remains constant, yet each tested value of *teta* yields a corresponding H_{Num} value, resulting in a set of vertically aligned points on the graphs. In certain cases, the code does not converge, thereby limiting the number of plotted points. This aspect will be further examined in the robustness evaluation of the enhancements.

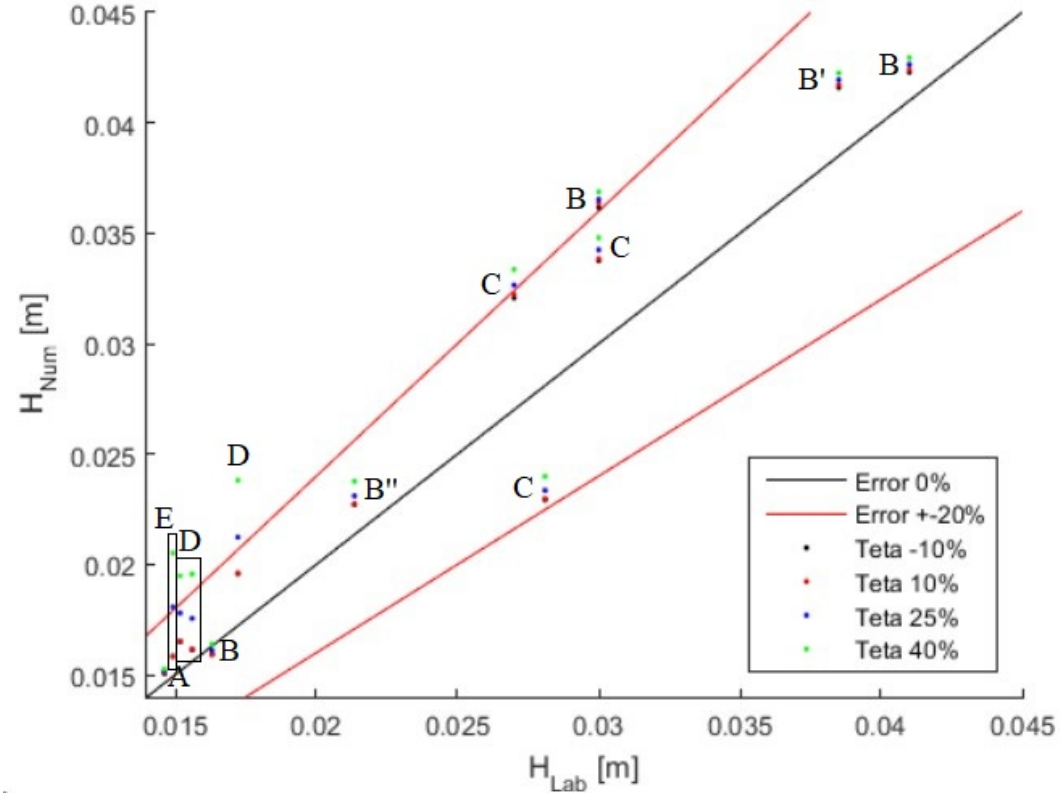

Figure 4.7: Impact of flow axis inclination within the outlet on the upstream head - Low head, reduced database (A = lowest θ_i, B = low θ_i, C = medium θ_i, D = high θ_i, E = highest θ_i)

These figures offer several conclusions:

1. For models with a gently inclined inlet, the inclination of the flow axis within the inlet has minimal impact on the upstream head. Conversely, the scatter of points for configurations with a steeply inclined inlet highlights a significant influence of this modification on the code's accuracy.

2. Within the explored range of values, a greater inclination of the flow axis (upward) corresponds to a higher upstream head. However, given the tendency of the initial model ($\theta = 0\%\theta_i$, horizontal) to overestimate this headwater level and considering the range of inclinations tested (-10% to 50% of θ_i), this code modification primarily results in a deterioration of the numerical model's precision.

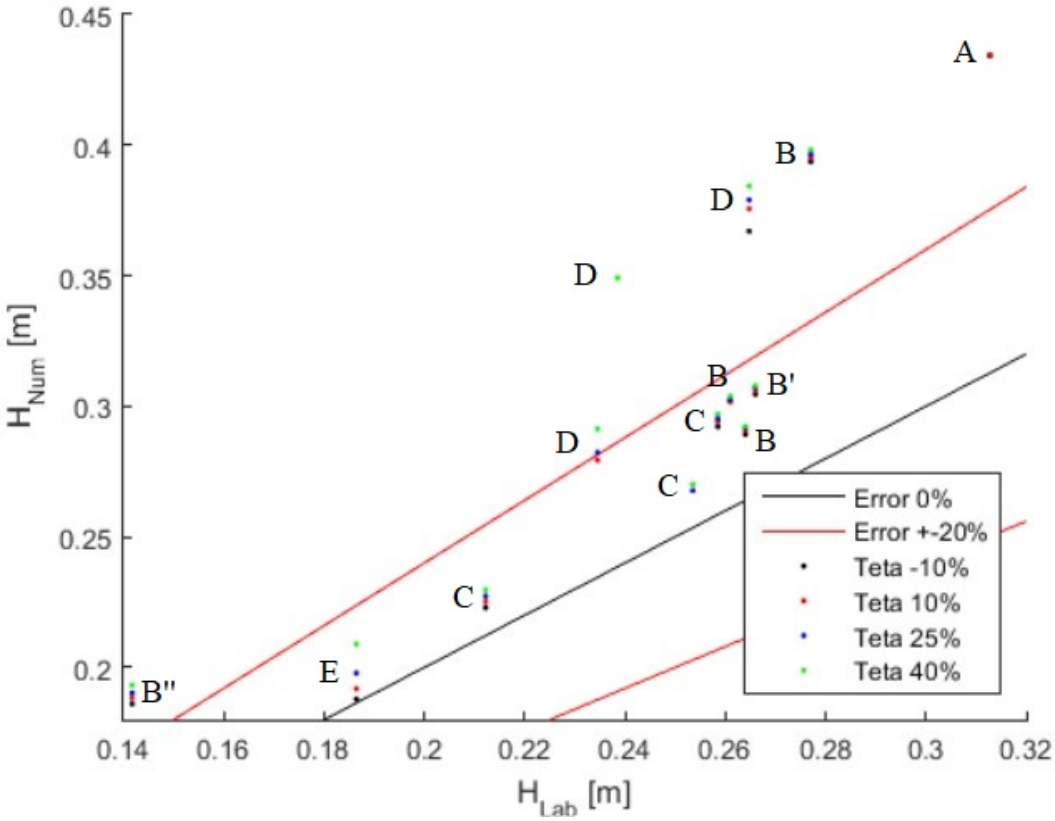

Figure 4.8: Impact of flow axis inclination within the outlet on the upstream head - High head, reduced database (A = lowest θ_i, B = low θ_i, C = medium θ_i, D = high θ_i, E = highest θ_i)

3. This trend, however, is less pronounced for small inclinations of the flow axis (the red and black points corresponding to $\theta = 10\%$ and -10% of θ_i are almost consistently overlapping). This observation prompts us to reconsider the choice of the lower bound for $\theta_{min} = -10\%\theta_i$, as we initially anticipated finding an optimum in upward flow inclinations, aligned with the bottom slope. The selection of a horizontally oriented flow axis, somewhat arbitrarily chosen in the first version of the code, could therefore be relatively sound.

4. The dispersion of results appears to be independent of the discharge and the initial error. These observations suggest that the inclination of the flow axis within the inlet may not be the primary hypothesis leading to the dominant error in the numerical model.

Tables 4.1 and 4.2 provide key statistics regarding the model errors for the full database. Tables 4.3 and 4.4 focus on the sample of configurations.

θ_i [as % of $\theta_{i,b}$]	*Mean error*	*Std deviation*	*Non − conv.*
−10%	+15.1%	+18.4%	20
10%	+16.1%	+18.7%	25
25%	+17.5%	+19.1%	29
40%	+19.8%	+19.5%	30

Table 4.1: Mean error and standard deviation of numerical error, and the number of non-converging simulations as a function of θ_i - Full database

Std deviation	*Q1*	*Q2*	*Q3*	*Q4*	*Q5*
$\theta_i = -10\%$	+11.8%	+18.7%	+20.1%	+19.8%	+17.8%
$\theta_i = 10\%$	+11.8%	+18.8%	+20.1%	+19.8%	+18.7%
$\theta_i = 25\%$	+12.1%	+19.1%	+20.1%	+20.1%	+20.1%
$\theta_i = 40\%$	+13.6%	+19.8%	+20.9%	+20.9%	+20.0%
Non − conv.	5	4	17	26	52

Table 4.2: Standard deviation of numerical error as a function of θ_i and upstream discharge - Full database

θ_i [as % of $\theta_{i,b}$]	*Mean error*	*Std deviation*	*Non − conv.*
−10%	+15.4%	+14.8%	3
10%	+16.7%	+14.9%	3
25%	+17.6%	+14.3%	4
40%	+20.7%	+15.3%	4

Table 4.3: Mean error and standard deviation of numerical error, and the number of non-converging simulations as a function of θ_i - Reduced database

Std deviation	*Q1*	*Q2*	*Q3*	*Q4*	*Q5*
$\theta_i = -10\%$	+9.9%	+15.8%	+15.3%	+15.2%	+15.3%
$\theta_i = 10\%$	+10.0%	+15.9%	+14.9%	+15.3%	+14.7%
$\theta_i = 25\%$	+12.4%	+16.4%	+14.9%	+13.9%	+14.1%
$\theta_i = 40\%$	+15.3%	+17.7%	+15.2%	+14.0%	+15.3%
Non − conv.	0	0	3	3	8

Table 4.4: Standard deviation of numerical error as a function of θ_i and upstream discharge - Reduced database

1.5 Results - second range

The third conclusion from the previous section prompted a new series of simulations. As the results for a strong inclination of flow in the inlet did not favor an improvement, the subsequent study focuses on flow directions with weaker inclinations, with a denser range of results covering inclinations between -10% and 10% of the bottom slope.

To begin, considering that trends differ at low and high flow rates, an analysis of each of these cases is undertaken separately.

On one hand, at low flow rates, a distinct minimum emerges. While previous simulations indicated a continuous growth of upstream head concerning the inclination of the flow direc-

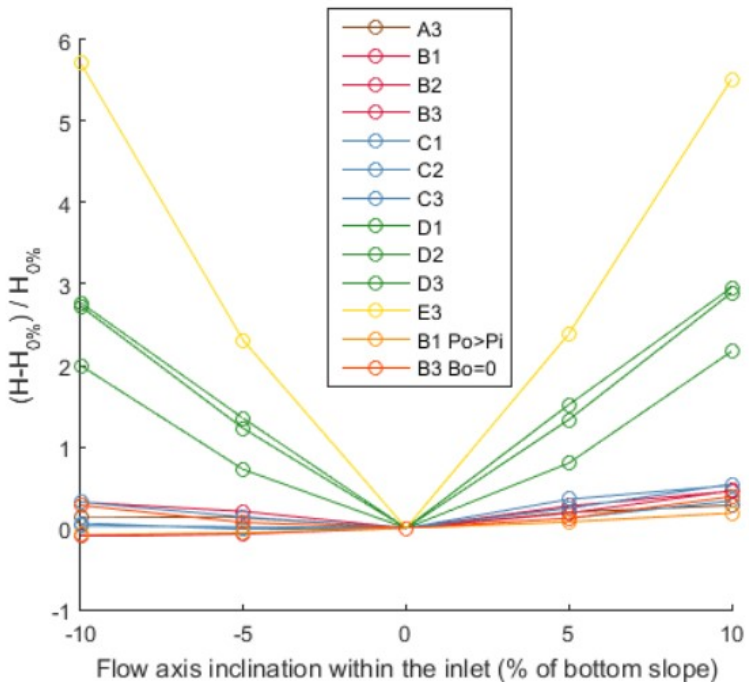

Figure 4.9: Impact of flow axis inclination within the outlet on the upstream head - Low head, reduced database (A = lowest θ_i, B = low θ_i, C = medium θ_i, D = high θ_i, E = highest θ_i)

tion (upward), Figure 4.9 showcases a minimum for a horizontal flow direction for nearly all selected configurations. Consequently, due to the systematic overestimation of the results by the numerical code, the initial intuition of maintaining a horizontal flow direction in the inlet seems to have been correct.

Another observation concerns the greater influence of the variable on the upstream head for configurations with steeper bottom slopes. However, this detail isn't particularly significant to retain, as the inclination of the flow direction is defined as a percentage of the bottom slope. Therefore, this merely underscores that a steeper inclination of the flow direction leads to a more pronounced impact on the upstream water depth.

Among the studied configurations, B1, B3, and B1' significantly deviate from the general trend. As illustrated in Figure 4.10, an upward flow direction contrarily induces a slight reduction in the upstream head, contrary to the rest of the observations.

On the other hand, as flow rate increases, the trend tends to align with the previously mentioned exceptions. Figure 4.11 portrays this evolution, starting from a scenario where a horizontal flow direction constitutes a minimum with relatively symmetric increase in upstream head concerning the inclination, and concluding with a consistent growth of water depth as the flow direction becomes more upward, accompanied by smaller variations in results. Depending on the configurations, this transition can be relatively gradual as flow rate increases. However, the shift from one trend to the other typically occurs abruptly at relatively low flow rates (e.g. A3).

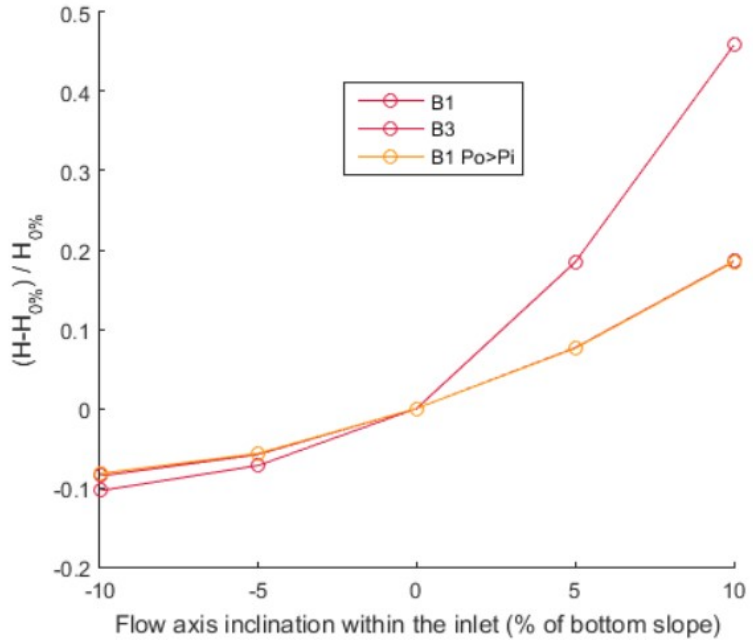

Figure 4.10: Impact of flow axis inclination within the outlet on the upstream head - Low head, reduced database (A = lowest θ_i, B = low θ_i, C = medium θ_i, D = high θ_i, E = highest θ_i)

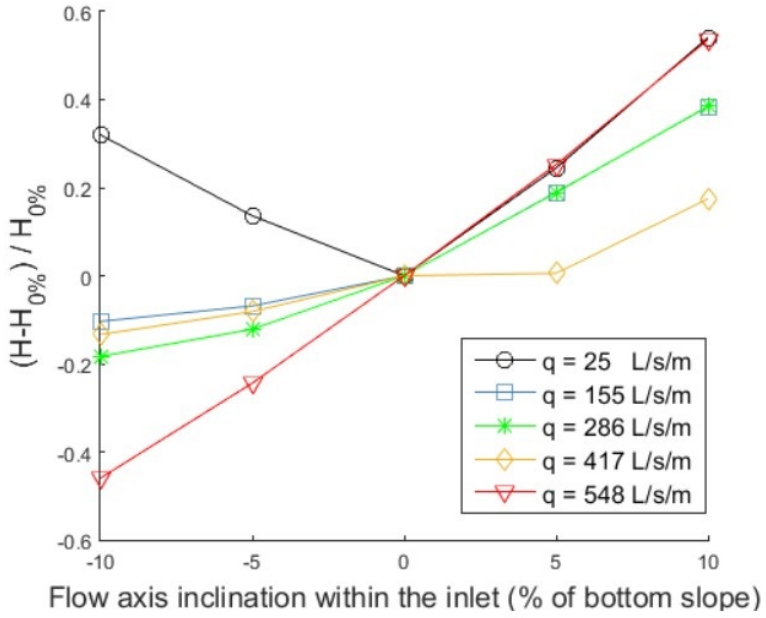

Figure 4.11: Impact of flow axis inclination within the outlet on the upstream head. Several discharges, Geometry 21 (D1)

The illustration of the previously described observations can be seen in Figure 4.11, thanks to the comparison with Figure 4.9. It should be noted that certain configurations are missing due to the non-convergence of certain results. It can also be noted that configuration B3 is still an exception at high discharge, with a growth of result higher at low head than at high head.

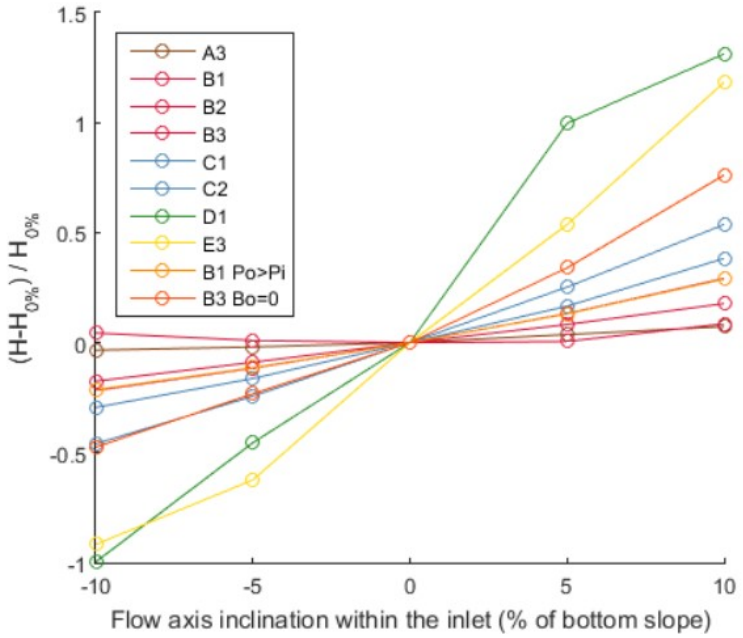

Figure 4.12: Impact of flow axis inclination within the outlet on the upstream head - Low head, reduced database (A = lowest θ_i, B = low θ_i, C = medium θ_i, D = high θ_i, E = highest θ_i)

1.6 Conclusion

This second sequence of simulations serves to refine the previously stated conclusion number 3:

3. At low flow rates, maintaining a horizontal flow axis within the inlet minimizes the upstream head, thereby improving the numerical model. At high flow rates, tilting the inlet flow axis downward can be physically justified and further reduces the upstream head, leading to error reduction. An optimal solution should involve an inlet flow inclination that is dependent on the incoming flow rate.

2 Lateral exchange : discharge coefficient of the lateral crest

2.1 Method for this sensitive analysis

One of the potential areas for improvement concerns the choice of the lateral discharge coefficient, $C_{w,Lat}$. As discussed in the preceding sections, this coefficient defines the lateral discharge based on the height of the flow.

This initial aspect regarding lateral exchanges is of paramount importance. On the one hand, the discharge capacity of the lateral crests constitutes the very essence of the comparative advantage of the PKW structures. On the other hand, the subsequent improvements pertain to lateral exchanges of momentum and the extraction and injection points of the two source terms related to these exchanges. All these variables are directly linked to mass exchange on the crests and, consequently, to this coefficient.

In the original version of the model, no recommendation was formulated for this coefficient. Article [26] merely cites the value "0.385 (thick crest)" without further justification.

However, the dataset available for this research work includes not only physical models from the University of ULiège laboratory with thick crests but also profiled crests with varying lateral crest curvature. As a result, both for this study and to provide a flexible tool for users, further consideration is required.

In the literature on lateral weirs, a recurring remark about this coefficient is that it is affected by the height of the flow, its velocity, and the orientation of the flow, a variable likely to vary along the crest [3]. Thus, numerous authors propose formulas involving these variables.

However, the 1D modeling only allows the definition of the height of the flow. Due to the lack of additional data on this matter (see the perspectives section), the impact of this coefficient on the results is evaluated, but a more in-depth study is challenging. To address the issue of different geometries, theoretical values derived from the theory of weirs are used as references: 0.385 for a thick crest for the models from Uliège and 0.42 for profiled crests (from EDF and EPFL), conservatively associated with a thin crest.

To assess the sensitivity of this factor, Figure 4.13 calculates the relative deviation of the upstream heads (the model's output) between the value calculated by the model with the theoretical value derived from the aforementioned reasoning, and the calculated value, this time, with a multiplier coefficient applied to the lateral discharge coefficient. This multiplier coefficient has been arbitrarily chosen as 130%. This method has been applied to the subset of configurations detailed earlier.

$$Variable = \frac{H(1.3 \times C_{w,lat,theorique}) - H(C_{w,lat,theorique})}{H(C_{w,lat,theorique})} \tag{2.1}$$

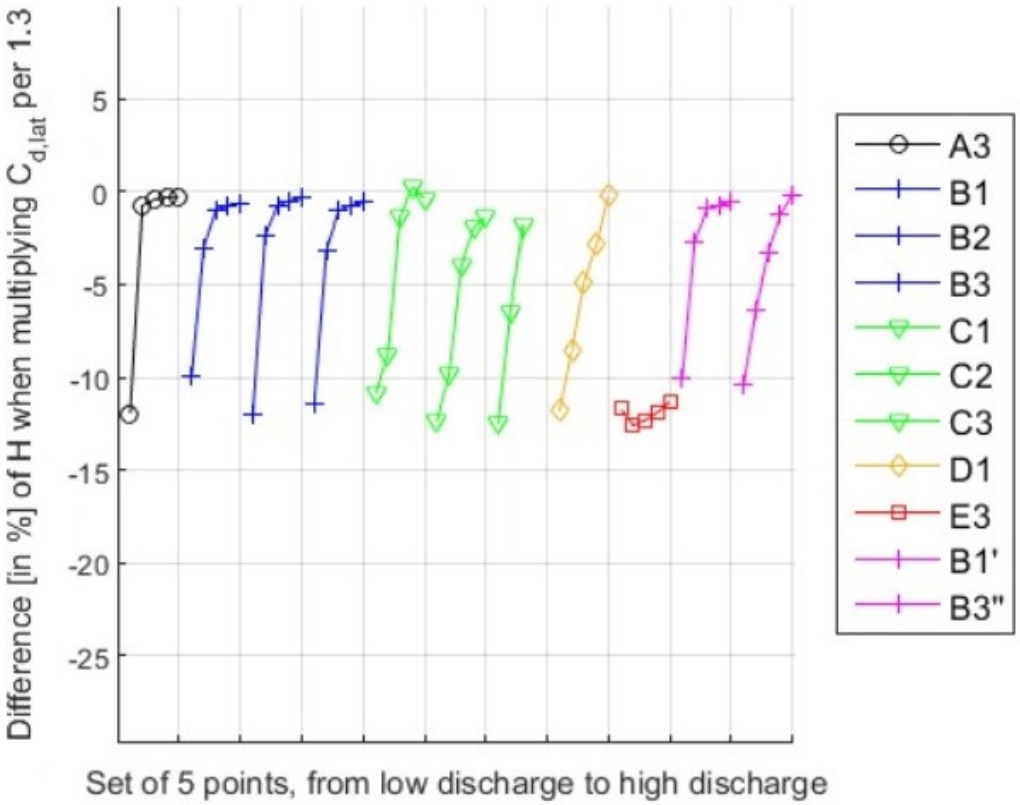

Figure 4.13: Sensitive analysis of the lateral discharge coefficient - reduced database (A = lowest θ_i, B = low θ_i, C = medium θ_i, D = high θ_i, E = highest θ_i) (1 = low W_i/W_o, 2 = medium W_i/W_o, 3 = high W_i/W_o)

2.2 Results

Two observations emerge from this analysis.

The first observation is the reduction in the influence of the lateral discharge coefficient with increasing upstream head, for all selected configurations (approximately -13% at low upstream flow rate compared to -0% at high upstream flow rate, except for E3). This result is fully explained by the physical understanding of the flow over the PKW structures. At low load, the lateral crests operate at full capacity with lateral flow perpendicular to the crest and a fully unobstructed outlet. Conversely, at high load, the inertia of the flow in the inlet induces a less optimal outflow angle (the flow is no longer locally perpendicular to the lateral crests), and the free surface in the outlet is much higher, reducing the difference in free surface on either side of the lateral crests. The discharge capacity is much less influenced by lateral exchanges and more strongly influenced by the flow rate over the frontal crests at the inlet's start and the

outlet's end.

The second observation is the slight difference in trends among the configuration classes. For geometries with very low slope in the inlet, this loss of influence is abrupt and occurs at relatively low upstream flow discharges. Conversely, for geometries with a steep slope in the inlet, the relationship between relative deviation and flow rate tends toward linear dependence. The same applies to configuration B3" without an upstream overhang.

One potential explanation for this result from a physical perspective would be related to the slope of the outlet's bed, not the inlet's. These slopes are generally opposite in the absence of a parapet. Thus, an outlet with a steeper bed slope will become less saturated, its significant slope providing both more volume for flow and a bed slope term more conducive to rapid flow. To borrow from O. Machiels' description [1], the PKW's inlet acts as the engine, and the outlet is the limiting constraint. This reasoning would suggest that geometries with a lower W_i/W_o ratio (Class 1) also have less restrictive outlets, and a distinction should appear between geometries with different width ratios for a similar inclination. However, this is not confirmed graphically.

From this analysis, it can be concluded that the impact of the lateral coefficient primarily results in a significant variation in the upstream head at low inflow discharges, while the variation becomes less pronounced at higher inflow discharges. This reduction in variation is even more pronounced for models with steeper inlet slopes. Since the primary model error occurs at high inflow discharges, this parameter does not appear to be the main weakness of the model. Moreover, due to the lack of information regarding the flow affecting the lateral discharge, calibrating the model through adjustments to this coefficient does not seem more relevant than a purely mathematical and non-physical statistical calibration. As such, this avenue of improvement will not be pursued for model calibration.

The model's precision exhibited greater accuracy for geometries stemming from laboratory tests conducted at EPFL and EDF (see Section 5.6). However, in these initial experiments, a distinct lateral discharge coefficient had been adopted in comparison to the geometries from the ULiège laboratory, due to the differing crest profiling. As demonstrated by Tables 3.1 and 3.2, configurations B1, B3, C1, C2, C3, and B1' originate from EPFL, B3" from EDF, and the remaining from ULiège. The influence of an augmentation in the lateral discharge coefficient does not appear to be heavily reliant on the initial value of this coefficient. Therefore, the preceding analysis retains its validity despite these disparities.

Nevertheless, this does not yet provide a justification, either in favor or against, for the relevance of distinguishing this lateral discharge coefficient based on the lateral crest shape.

2.3 Conclusion

In summary, the two primary observations can be summarized as follows:

5. An increase in the lateral discharge coefficient consistently results in a reduction of upstream head, as lateral flow constitutes a significant component of the PKW discharge.

6. The impact of this parameter diminishes as the flow rate increases. This reduction in influence is abrupt for low bed slopes, becoming more linear for configurations with steeper upstream bed slopes.

3 Lateral exchange : the α coefficient from the momentum equation

3.1 Modification of the model and sensitive analysis

As discussed earlier, the coefficient α characterizes the momentum transfer during lateral exchange between the inlet and outlet. The model initially set this coefficient to 1 for both the inlet and the outlet. Additionally, the transferred momentum is calculated in a manner that does not alter the momentum per unit mass of the considered flow (Equation 5.2). Thus, the momentum taken from the inlet by a lateral flux does not equate to the momentum introduced at the outlet by the same lateral flux.

Consequently, two distinct improvements have been examined regarding this momentum exchange term.

The first improvement stems from the model's flow conservation principle. By decoupling the momentum quantities extracted from one water line and transferred to the neighboring water line, the modeler relinquishes control over the generated or lost momentum during the exchange.

In the majority of cases, the average water height at the inlet surpasses the average water height at the outlet, leading to an exchange of mass and momentum from the inlet to the outlet. However, at high flow rates, particularly in the upstream portion of the lateral crest, this relationship may reverse. Nonetheless, observations demonstrate that even in these atypical cases, lateral fluxes are oriented from the inlet to the outlet.

Hence, the code connects the momentum flux extracted from the inlet and introduced at the outlet, calculating this momentum quantity solely based on the longitudinal flow velocity

in the inlet. Equation 5.2 is thus transformed into:

$$S_{l,j} = \alpha_j \underline{u_{x,1}} \cdot \underline{e_{x,j}} \tag{3.1}$$

The second avenue for improvement pertains to the selection of the α coefficient. As explained in the initial part of this study, no quantitative data systematically assesses the orientation of lateral flux, drop, and head loss during the blending of lateral and longitudinal flows. Consequently, while it would have been ideal to define an α coefficient dependent on these characteristics and thus variable throughout the simulation (from finite volumes to finite volumes and from time step to time step), the dearth of supplementary data favored a less complex sensitivity analysis.

Thus, the range of values originates from physics and remains, as previously described, $\alpha \in [0, 1]$. This range is discretized into 6 equidistant points for sensitivity analysis. For the 13 selected configurations and the five flow rates per geometry, this corresponds to 390 simulations to be conducted.

On the other hand, differentiating this parameter between the inlet and outlet ($\alpha_1 \neq \alpha_2$) could be insightful, but its physical interpretation is intricate. The drop tends to generate momentum during transfer, leading to $\alpha_1 < \alpha_2$, whereas head loss due to the mixing of flows at the outlet has the opposite effect. In the absence of supplementary data, the choice to not differentiate coefficients between the inlet and outlet ($\alpha_1 < \alpha_2$) is maintained for sensitivity analysis.

3.2 Results of the sensitive analysis

The results from this sensitivity analysis exhibit trends that are less distinctive than those observed in the analysis of the flow axis inclination. Nevertheless, several observations can still be made.

Indeed, Figure 4.14 clearly demonstrates the reduction in upstream head by selecting a lower coefficient α. This implies that at low flow rates, retaining a maximum amount of momentum in the inlet enhances the spillway discharge. This rationale aligns with the fact that, at low flow rates, the flow in the outlet proceeds unhindered, making the outlet a non-limiting factor. However, the inlet, described as the "engine" of the flow over the PKW [1], possesses a greater amount of momentum, thereby increasing the discharge or, for a fixed upstream flow rate, reducing the upstream head of the PKW.

The impact of the bed slope on the enhanced discharge for lower α coefficients is more complex to interpret. Graphically, and still at low upstream flow rates, the dispersion of results appears to be highest for intermediate bed slope classes (B and C) and markedly reduced for steeper bed slopes. Figure 4.16 provides a clearer depiction of this outcome, showing variations of up to 10% for intermediate classes compared to less than 5% for higher classes.

The configuration without an upstream overhang also stands out with a significant variation at low flow rates, exhibiting a 12% change in upstream head when transitioning from $\alpha = 1$ to $\alpha = 0$.

However, this trend is not upheld across all configurations.

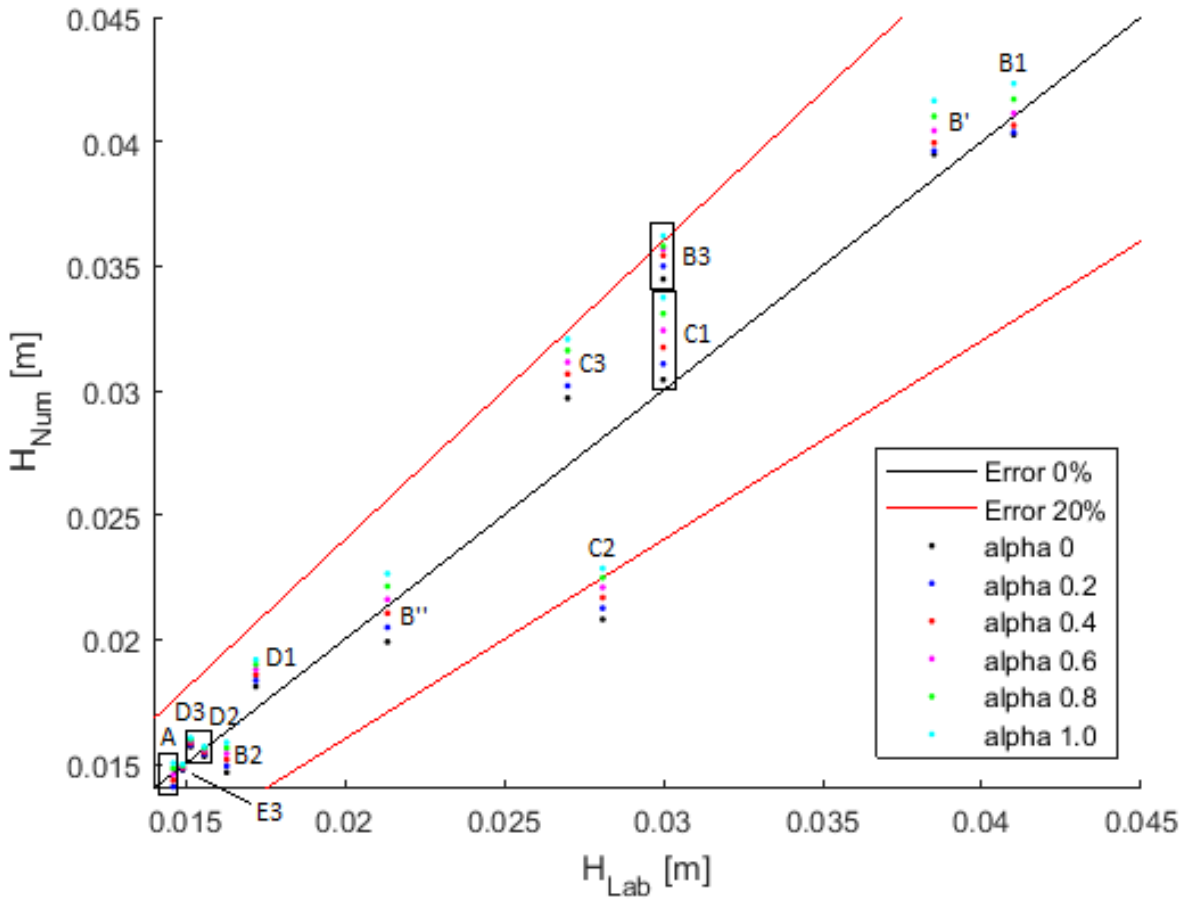

Figure 4.14: Sensitive analysis of the α coefficient - Low head, reduced database (A = lowest θ_i, B = low θ_i, C = medium θ_i, D = high θ_i, E = highest θ_i)

However, this trend does not persist across all levels of flow. As depicted in Figure 4.15, the relative proportionality between upstream head and the alpha coefficient eventually undergoes inversion. A reduction in the coefficient leads, at higher flow rates, to an increase in upstream head. Some configurations, particularly those with steeper bed slopes, deviate from this rule, notably the E3 configuration.

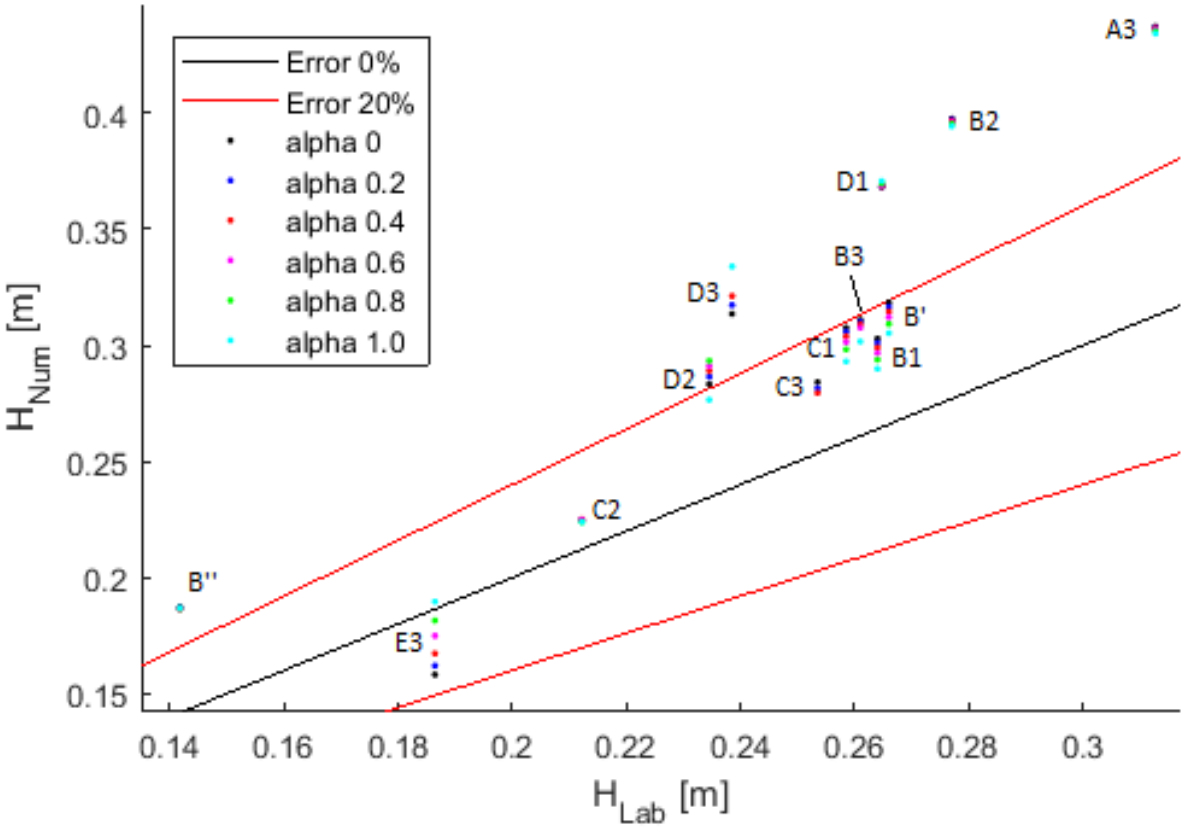

Figure 4.15: Sensitive analysis of the α coefficient - High head, reduced database (A = lowest θ_i, B = low θ_i, C = medium θ_i, D = high θ_i, E = highest θ_i)

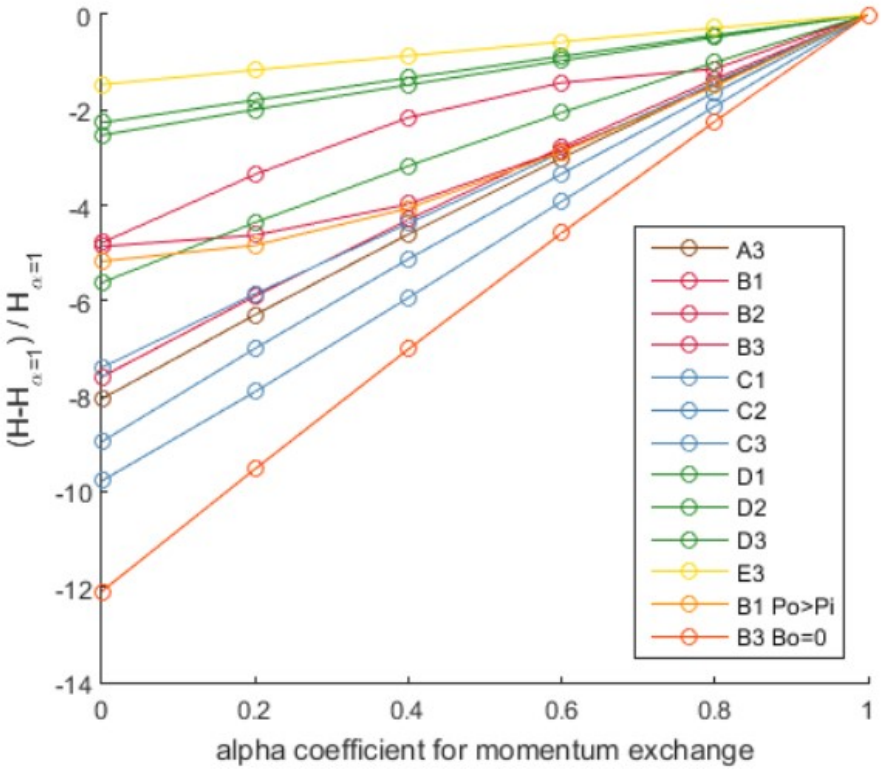

Figure 4.16: Sensitive analysis of the α coefficient - Q1, reduced database (A = lowest θ_i, B = low θ_i, C = medium θ_i, D = high θ_i, E = highest θ_i)

To gain deeper insights into the potential reversal of this trend, Figures 4.17, 4.18, and 4.19 provide results for flow rates Q2, Q3, and Q4. These figures demonstrate that the transition can occur progressively (as seen in configurations D) or in an abrupt manner, such as with the configuration lacking an upstream overhang, which shifts from a -12% change (between $\alpha = 1$ and $\alpha = 0$) at the lowest flow rate to a +12% change in the subsequent flow rate.

In general, the curves tend to converge at higher flow rates, indicating a less significant impact of this coefficient on the upstream head of the PKW. This could be understood similarly to lateral mass flow exchanges, as these lateral flows become less dominant at high flow rates, diminishing the influence of parameters related to their modeling as the flow increases.

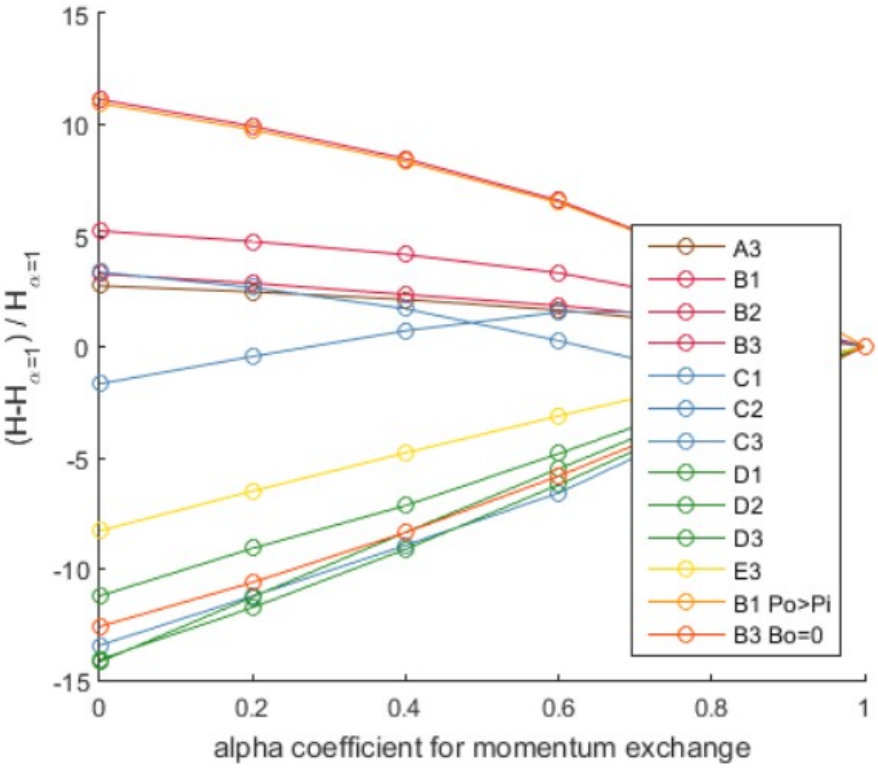

Figure 4.17: Sensitive analysis of the α coefficient - Q2, reduced database (A = lowest θ_i, B = low θ_i, C = medium θ_i, D = high θ_i, E = highest θ_i)

Tables 4.5 and 4.6 provide key statistics regarding the model errors.

3.3 Conclusion

The initial model, operating with $\alpha = 1$, exhibited increasing numerical overestimation with respect to the inflow discharge. Consequently, this overestimation could be significantly mitigated at low discharges, as illustrated by the errors depicted in Figure 4.14 for $\alpha = 1$. However, Figure 4.15 reveals the limitations of this improvement at higher discharges. As reducing the alpha coefficient leads to a relatively smaller increase in upstream head, this augmentation

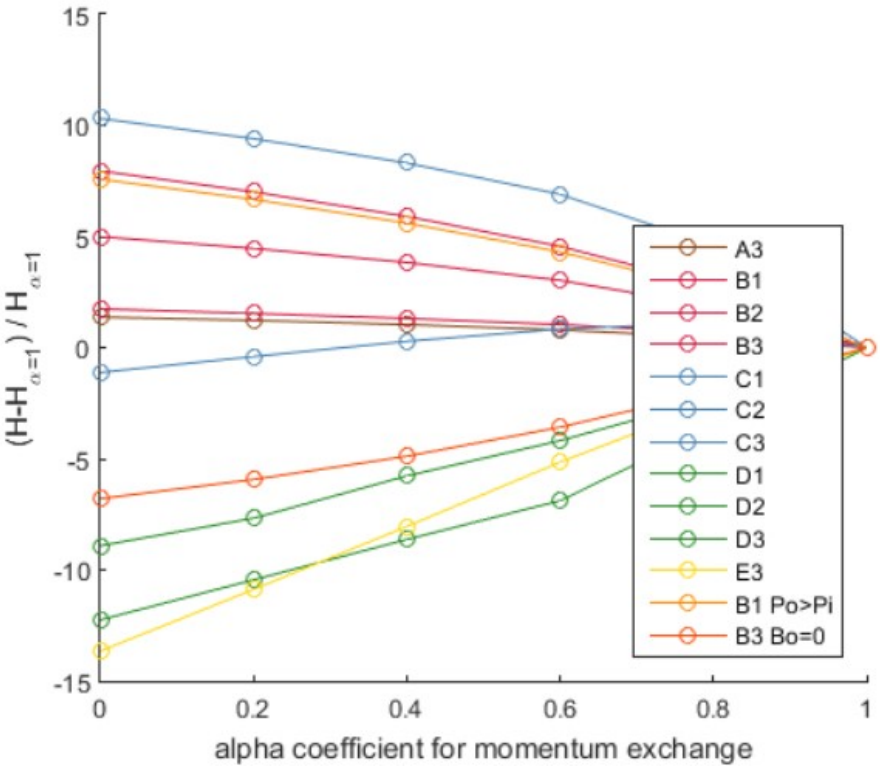

Figure 4.18: Sensitive analysis of the α coefficient - Q3, reduced database (A = lowest θ_i, B = low θ_i, C = medium θ_i, D = high θ_i, E = highest θ_i)

α	*Mean error*	*Std deviation*	$Non-conv.$
0	+13.5%	+17.2%	3
0.2	+14.1%	+16.6%	3
0.4	+14.8%	+16.0%	2
0.6	+15.5%	+15.7	3
0.8	+15.2%	+15.2%	6
1	+16.1%	+15.1%	2

Table 4.5: Mean error and standard deviation of numerical error, and the number of non-converging simulations as a function of θ_i - Reduced database

Std deviation	*Q1*	*Q2*	*Q3*	*Q4*	*Q5*
$\alpha = 0$	+10.0%	+17.5%	+17.0%	+16.1%	+16.0%
$\alpha = 0.2$	+10.0%	+16.8%	+16.7%	+15.5%	+15.8%
$\alpha = 0.4$	+10.0%	+16.1%	+15.5%	+15.3%	+15.5%
$\alpha = 0.6$	+9.9%	+15.8%	+15.0%	+15.7%	+15.3%
$\alpha = 0.8$	+9.9%	+15.6%	+15.3%	+14.6%	+15.7%
$\alpha = 1$	+10.0%	+15.7%	+15.2%	+15.0%	+15.0%
$Non-conv.$	0	0	0	1	1

Table 4.6: Standard deviation of numerical error as a function of θ_i and upstream discharge - Reduced database

exacerbates the numerical model's overestimation.

These recent developments can be summarized as follows:

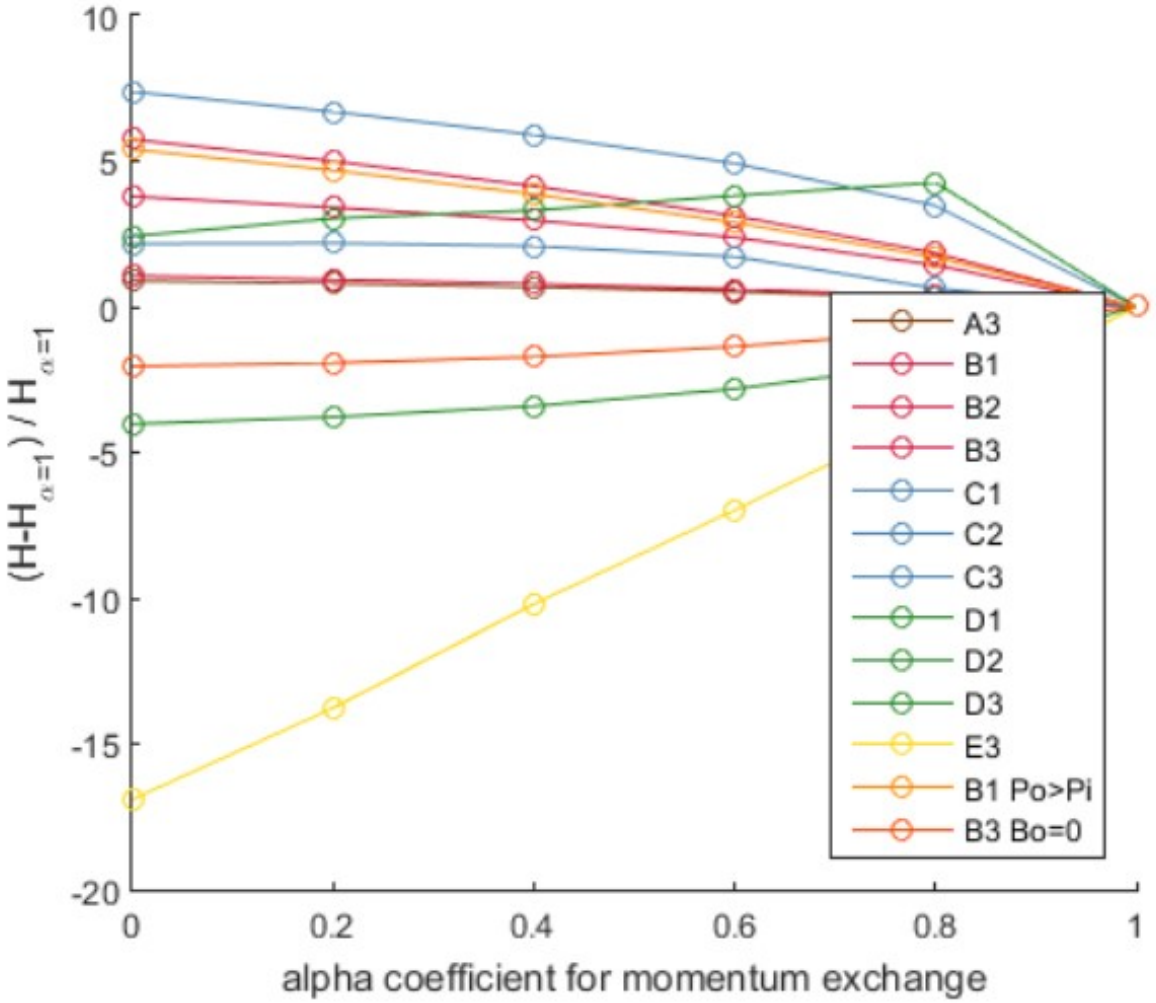

Figure 4.19: Sensitive analysis of the α coefficient - Q4, reduced database (A = lowest θ_i, B = low θ_i, C = medium θ_i, D = high θ_i, E = highest θ_i)

7. At low discharge rates, any reduction of the alpha coefficient allows for a substantial reduction in head, sufficiently counterbalancing the numerical model's overestimation for the extreme scenario $\alpha = 0$. The influence of this parameter appears to be more pronounced for intermediate bed slopes.

8. At high discharge rates, the trend stated in point 7 is reversed: reducing the alpha coefficient results in an increase in the numerical overestimation of upstream head. Nevertheless, the correlation between alpha and upstream head is less significant than at low discharge rates due to the diminishing influence of lateral spill flows.

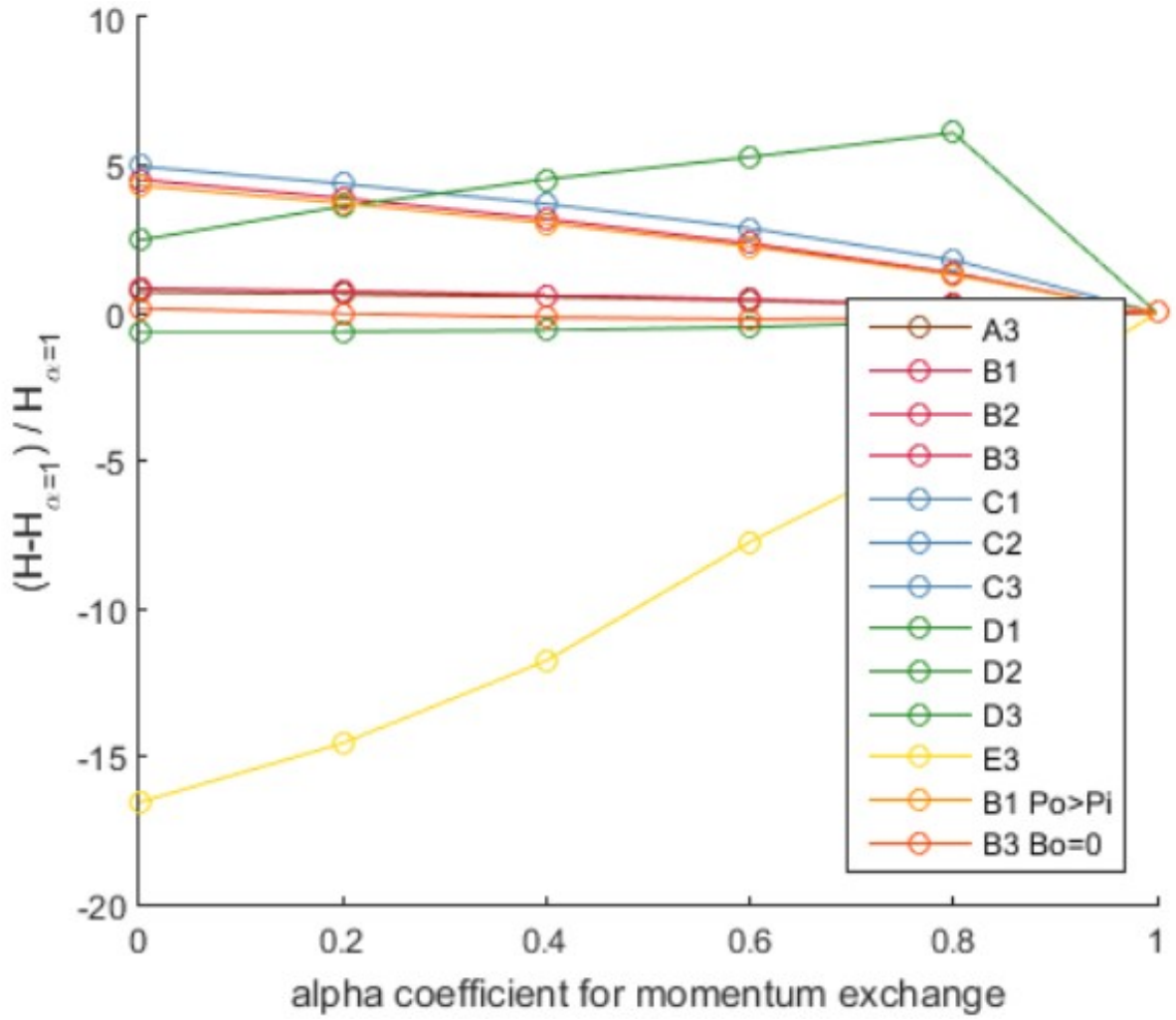

Figure 4.20: Sensitive analysis of the α coefficient - Q5, reduced database (A = lowest θ_i, B = low θ_i, C = medium θ_i, D = high θ_i, E = highest θ_i)

4 Lateral exchange : the locations for lateral flux extraction and injection

4.1 Physical and experimental rationale

Figure 2.15 illustrates how the free surface of each of the two water lines is computed to calculate mass exchanges using Equation 3.4. However, despite the required projection for the free surface calculation, lateral exchange is simply extracted and injected into the volumes with their horizontal abscissae at the projected abscissa. As a result, the volume at the origin of the free surface is not necessarily the one exchanging the calculated flux. This choice is understandable due to the relatively simplified modeling, but it raises questions about its physical validity.

Indeed, Figure 4.25 elucidates this issue regarding the inclination of one of the flow axes (in this case, that of the inlet). Depending on the direction of the axis inclination, the point of calculation for the free surface may be located upstream or downstream of the horizontal

abscissa of the free surface. Consequently, it seems justified to extract the lateral mass flux from a volume either upstream or downstream of this abscissa.

Therefore, this study explores the possibility of allocating the lateral flux to the volume at the origin of its calculation. This approach becomes even more relevant as the first idea explored is the inclination of the flow axis in the inlet. Given that of the outlet is already inclined, this would necessitate complicating the modeling for both the inlet and the outlet.

Another consideration pertains to the momentum possessed by the previously discussed lateral flow, an aspect also explored in idea 3 concerning the alpha coefficient. As the lateral flow traverses the lateral weir crest, it exhibits varying outflow angles as shown in Figures 4.21 and 4.22.

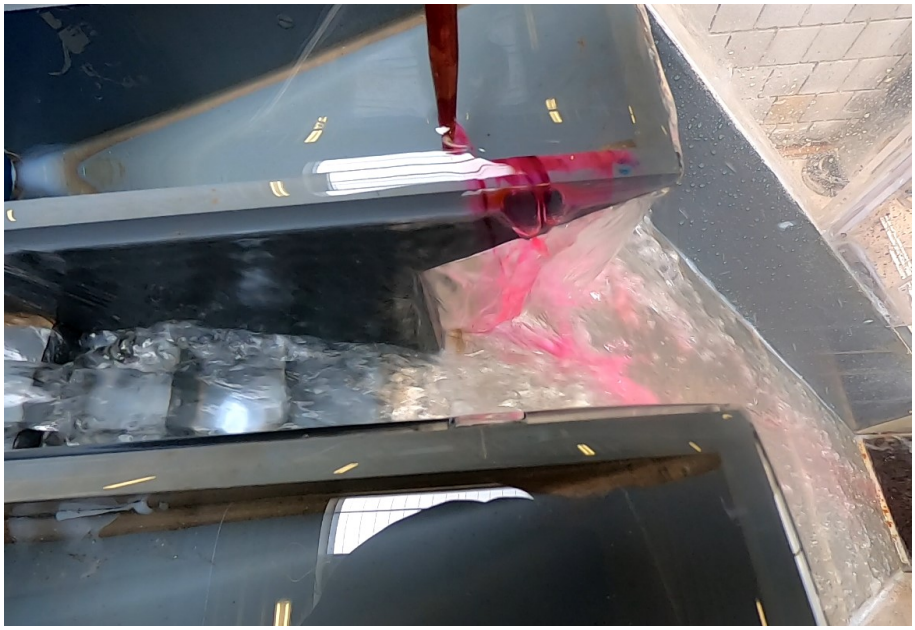

Figure 4.21: Uliège laboratory : flow's attack angle almost perpendicular to the lateral crest

At low discharge, the flow's attack angle is nearly perpendicular to the lateral crest. Figure 4.23 attempts to illustrate this observation, though a video format or laboratory observation would better convey it. An intriguing observation is also the variability of this attack angle along the crest, particularly with more oblique velocities in the extreme upstream zone of the lateral crest.

This absence of momentum would entail a relatively straightforward choice for horizontal flow axes: the original model, where all lateral terms are calculated, extracted, and injected using vertical projection.

Conversely, at higher discharges, the attack angle gradually diminishes. Flow velocities in the inlet intensify, increasing the flow's inertia and imparting a progressively more significant

Figure 4.22: Uliège laboratory : flow's attack angle at about 45° to the lateral crest

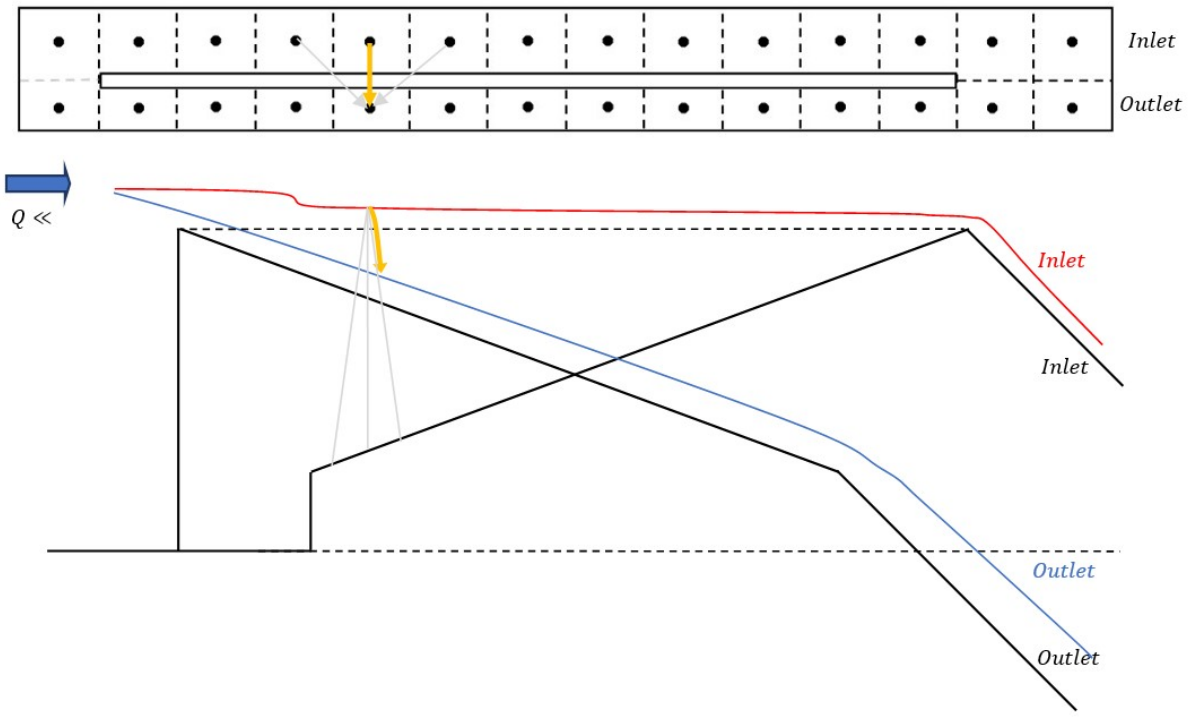

Figure 4.23: Lateral discharge term with different main flow axis in the inlet and in the outlet

momentum to the lateral flow. Due to the potential drop this lateral flow may experience after crossing the crest, it might only join the inlet flow downstream of the crest's passage point. Thus, even without considering longitudinal flow axis inclination, the extraction abscissa for the flux might differ from its injection point, as depicted in Figure 4.24.

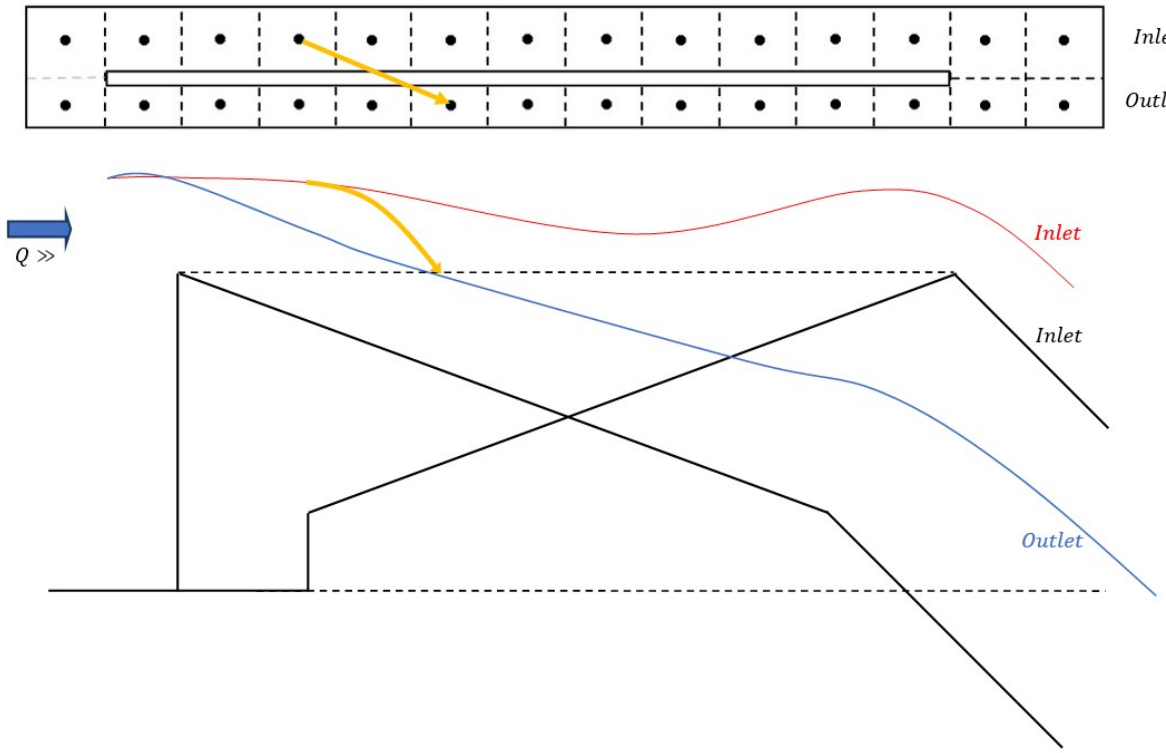

Figure 4.24: Lateral discharge term with different main flow axis in the inlet and in the outlet

4.2 Implementation

Given the domain discretization, a challenge that promptly arises during the implementation phase is determining where to extract and where to inject if the projected abscissa falls between two finite volume centers of gravity.

Indeed, as the inclination of the flow axes is not always constant along the inlet and outlet, as aptly illustrated by Figure 4.5, conflict zones emerge. The lateral discharge calculated at a particular horizontal abscissa is then distributed among various volumes projecting their free surface in that part of the domain. For the generic example depicted in Figure 4.25, the lateral discharge calculated for abscissa i can be divided as follows:

$$\begin{aligned} Q_{lat,i-3} &= \tfrac{a}{a+b} Q_{lat,i} \\ Q_{lat,i-2} &= \tfrac{b}{a+b} Q_{lat,i} \end{aligned} \tag{4.1}$$

Of course, it is necessary to temporarily store the initial lateral discharge values and then sum up the partial contributions, volume by volume. Equation 4.1 illustrates a relatively straightforward example where two volumes share a common lateral discharge. Due to the non-constant inclinations, it can occur that either 0 or 4 volumes share a discharge. The guiding principle in this endeavor is the conservation of mass, thus ensuring that all discharges are allocated only once.

Following this method, the lateral discharges are thus "connected." The lateral discharge in the inlet is no longer simply the opposite of the lateral discharge in the outlet at the corresponding abscissa. This change in implementation introduces slight oscillations in the model's convergence process.

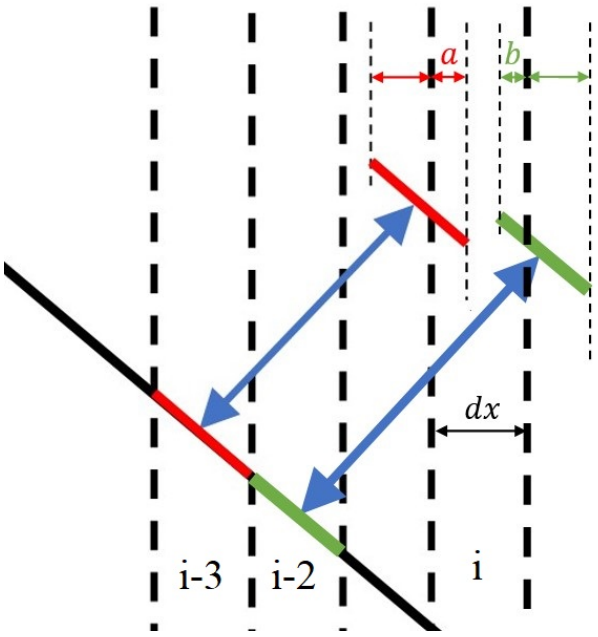

Figure 4.25: Distribution of lateral discharges among finite volumes projecting their free surface at similar abscissas.

This enhancement was successfully implemented and validated. However, an error introduced in the code violated the conservation of mass principle : distant abscissae from any projected free surface did not to attribute their lateral discharge to any cell, thus biasing the code's results. Since this error was detected relatively late in the development process, no results analysis could be conducted.

5 model robustness

Finally, the robustness of this model has also been enhanced.

The previous version of the code had an effective yet less rigorous signal processing approach in many cases. This method involved comparing the discharge difference between the inflow discharges of the two cells and the imposed boundary condition at regular intervals of iterations. If this difference fell below the tolerance threshold, the solution was deemed steady-state, and the upstream water level was provided as the output of the numerical model.

However, the initial version of the code did not converge for certain geometries, particularly at high upstream flow rates. Upon closer examination of the signal, it became apparent that for some configurations, the system oscillated between two states, never reaching a steady state. This oscillation is generally caused by the submergence of the outlet, which is more prone to convergence issues during simulations with high flow rates that are conducive to submergence. The flow dynamics are as follows: once the outlet becomes submerged, the water level in the inlet rises. This rise in water level reduces the water level differential between the inlet and outlet, thus decreasing the lateral discharge. This reduction then, in certain contexts, leads to an increase in the Froude number in the outlet, causing it to transition back to supercritical flow, thereby reducing its water level. This reduction triggers an increase in lateral discharge, which raises the Froude number and restarts the cycle.

These oscillations often manifest as a very small variation in the upstream water level. Thus, even though a steady state is not reached, the upstream water level becomes stabilized and could be provided as a result.

Furthermore, the various code improvements introduced some noise to this oscillatory signal. As such, a simplistic criterion was challenging to implement. The convergence criterion has thus been refined with more extensive signal processing, including the use of Fourier transforms to identify the frequency generating the majority of the oscillatory signal's amplitude. When the oscillation is stabilized, the upstream water level is provided as the result. The remaining amplitude of the signal serves as an estimation of the numerical error associated with this convergence criterion.

Chapter 5

Conclusions

1 General conclusion

During the course of this study, the limiting assumptions of the WOLF1DPKW model were critically examined, including:

2. Assuming a horizontal flow axis at the inlet despite an inclined bed slope;

3A. Employing a single lateral discharge coefficient for all geometries;

3D. Employing an overly simplified approach for computing free surfaces and the locations of lateral inflow and outflow, without considering the inclination of flow axes;

3B and C. Utilizing a highly simplistic momentum exchange modeling (alpha = 1).

Several key findings emerged concerning each of these assumptions.

Regarding the inclination of the axis at the inlet, the initially somewhat arbitrary choice was found to be appropriate. Specifically:

- An upward flow axis inclination at the inlet leads to an upstream load increase, thereby amplifying the model's overestimation of the load. This deterioration is more pronounced for steep models and, independently, for lower upstream flows.
- Conversely, a downward flow axis inclination shows a slight improvement at low flows and can be physically justified.

Concerning the lateral discharge coefficient:

- The lateral crest profiling differs between the laboratories, and theoretically, this discrepancy justifies the choice of a coefficient of 0.42 for profiled crests. This modification results in significantly lower errors for models with profiled crests compared to those with thick crests, across all flow levels.
- Increasing the coefficient from 0.385 to account for the thick crests of ULiège's models proves to be of limited use in reducing the error at high flow levels.

Regarding the alpha coefficient:

- Several physical considerations warrant a more complex treatment of this parameter, involving volume-by-volume and time-step-by-time-step calculations instead of being constrained to a constant parameter throughout the simulation, shared equally by the inlet and outlet.
- The impact of this parameter on model correction varies considerably from one configuration to another and based on flow rates. The effect of transitioning from $\alpha = 1$ to $\alpha = 0$ fluctuates between +10% and -10% on upstream load, contingent on the context.

2 Prospects for improvement

Throughout this study, ideas for further analysis have emerged. Here is a list of complementary research avenues that could deepen the analysis and refine the results:

- The notion of accounting for spaces beneath the overhangs in the WOLF1DPKW model has not been explored in this work. As this aspect has been identified as a potentially significant limitation of the model, its analysis could help elucidate certain numerical errors that could not be adequately rectified.
- Each sensitivity analysis was conducted relatively independently in this report. However, a portion of the simulations conducted during this work comprehensively mapped all possible parameter combinations within the specified ranges. These data could serve as a solid starting point for a proper calibration of the numerical model.
- A substantial portion of the reflections on flow physics, such as the differentiation of parameters in spatial and temporal domains or the evolution of these parameters based on discharge, offer promising paths for refining the model. To maintain an approach firmly rooted in physics while calibrating the model as accurately as possible, specific measurements could be taken using physical scaled-down models or 3D modeling. For instance, measurements on the angle of attack of lateral exchange flows could refine the range choices that make physical sense for the α coefficient.

- The sampled database focused on the relative height of PKWs and the inlet/outlet width ratio. A similar analysis could be conducted by concentrating on the upstream and downstream overhang length ratio, the impact of parapets, crest thickness, or even the L/W ratio.

Furthermore, all these analyses assume relatively standard geometries on certain aspects. The currently constructed PKWs exhibit geometric specifics such as stepped outlet slopes, rounded or chamfered corners of the "piano keys." These modifications could play a significant role in flow dynamics and impact the conclusions of this work.

Finally, this study has centered on reducing the error of a model. A comparative analysis of pre-sizing models and their accuracy, using a shared database, could evaluate the relevance of this improved model.

Bibliography

1 Machiels, O. (2012). Experimental study of the hydraulic behaviour of Piano Key Weirs.

2 Johnson, M. C. (2000). Discharge coefficient analysis for flat-topped and sharp-crested weirs. Irrigation science, 19, 133-137.

3 Hager, W. H. (1987). Lateral outflow over side weirs. Journal of Hydraulic Engineering, 113(4), 491-504.

4 Blanc, P., & Lempérière, F. (2001). Labyrinth spillways have a promising future. International Journal on Hydropower & Dams, 8(4), 129-131. International Journal on Hydropower & Dams 8.4 (2001), pp. 129–131.

5 Lempérière, F. (2009). New Labyrinth weirs triple the spillways discharge–Data for an easy design of PK Weir. Available online on www. hydrocoop. Org.

6 Laugier, F. (2007). Design and construction of the first Piano Key Weir spillway at Goulours dam. International Journal on Hydropower & Dams, 14(5), 94-100.

7 Bieri, M., Federspiel, M., Boillat, J. L., Houdant, B., & Delorme, F. (2009). Spillway capacity upgrade of Gloriettes dam: environmental integration and energy dissipation. Proceedings of HYDRO 2009" Progress–Potential–Plans ".

8 Cicéro, G. M., Guene, C., Luck, M., Pinchard, T., Lochu, A., & Brousse, P. H. (2010, May). Experimental optimization of a Piano Key Weir to increase the spillway capacity of the Malarce dam. In 1st IAHR European Congress, Edinbourgh, 4–6 mai 2010.

9 Dugué, V., Hachem, F., Boillat, J. L., Nagel, V., Roca, J. P., & Laugier, F. (2011, May). PKWeir and flap gate spillway for the Gage II Dam. In Proc. Int. Conf. Labyrinth and Piano Key Weirs Liège B (pp. 35-42).

10 Erpicum, S., Laugier, F., Boillat, J. L., Pirotton, M., Reverchon, B., & Schleiss, A. J. (Eds.). (2011). Labyrinth and piano key weirs. CRC press.

11 Erpicum, S., Machiels, O., Archambeau, P., Pirotton, M., & Dewals, B. (2012). Hydraulic modelling of Piano Key Weirs: a composite approach. In International workshop on Piano Key Weir for In-stream Storage and Dam Safety-PKWISD-2012.

12 Laugier, F., Lochu, A., Gille, C., Leite Ribeiro, M., & Boillat, J. L. (2009). Design and construction of a labyrinth PKW spillway at Saint-Marc dam, France. Hydropower & Dams, 16(ARTICLE), 100-107.

13 Laugier, F., Vermeulen, J., & Pralong, J. (2012). Achievement of new innovative labyrinth piano key weir spillways (PKW). Proceedings of piano key weir for in-stream storage and dam safety (pKwIsD-2012), New Delhi. New Delhi, India, 25-42.

14 Ribeiro, M. L., Boillat, J. L., Schleiss, A., Laugier, F., & Albalat, C. (2007). Rehabilitation of St-Marc dam. Experimental optimization of a piano key weir. In Proc. of 32nd Congress of IAHR. Vince. Italy.

15 Leite Ribeiro, M., Boillat, J. L., Kantoush, S., Albalat, C., Laugier, F., & Lochu, A. (2007). Rehabilitation of St-Marc dam: Model studies for the spillways (No. CONF).

16 Pinchard, T., Farges, J. L., Boutet, J. M., Lochu, A., & Laugier, F. (2013). Spillway capacity upgrade at Malarce dam: Construction of an additional piano key weir spillway. Labyrinth and Piano Key Weirs, 243-252.

17 Da Singhal, G., & Sharma, N. (2011, May). Rehabilitation of Sawara Kuddu Hydroelectric Project–Model studies of Piano Key Weir in India. In Proc. Intl Workshop on Labyrinths and Piano Key Weirs PKW 2011 (pp. 241-250).

18 Khanh, H. T. (2011). M., Sy Quat, D., Xuan Thuy, D. 2011a. PK weirs under design and construction in Vietnam. In Proc. Intl Workshop on Labyrinths and Piano Key Weirs PKW 2011 (pp. 225-232).

19 Khanh, M. H. T. (2013). The Piano Key Weirs: 15 years of Research & Development–Prospect. Labyrinth and piano key weirs II, 3.

20 Sharma, N., & Das Singhal, G. (2012). Physical modelling of Piano Key Weir for Sawra Kuddu Hydro Electric Project in India. Piano Key Weir for in-stream storage and dam safety (PKWISD-2012), 123-132.

21 Erpicum, S., Machiels, O., Dewals, B., Archambeau, P., & Pirotton, M. (2010). Contribution to the study of Piano Key Weir hydraulics. In 8th ICOLD European Club Symposium. ATCOLD.

22 Erpicum, S., Machiels, O., Archambeau, P., Dewals, B., Pirotton, M., & Daux, C. (2011). Energy dissipation on a stepped spillway downstream of a Piano Key Weir–Experimental study. Labyrinth and Piano Key Weirs I-PKW 2011, 105-112.

23 Erpicum, S., Machiels, O., Dewals, B., Pirotton, M., & Archambeau, P. (2012). Numerical and physical hydraulic modelling of Piano Key Weirs. In Asia 2012-4th Int. Conf. on Water Resources and Renewable Energy Development in Asia.

24 Tullis, J. P., Amanian, N., & Waldron, D. (1995). Design of labyrinth spillways. Journal of hydraulic engineering, 121(3), 247-255.

25 Pralong, J., Vermeulen, J., Blancher, B., Laugier, F., Erpicum, S., Machiels, O., ... & Schleiss, A. J. (2011, May). A naming convention for the Piano Key Weirs geometrical parameters. In proceedings of the International Conference Labyrinth and Piano Key Weirs (pp. 271-278).

26 Erpicum, S., Machiels, O., Archambeau, P., Dewals, B., & Pirotton, M. (2010). 1D numerical approach to model the flow over a Piano Key Weir (PKW). In SimHydro 2010: Hydraulic modeling and uncertainty. SHF, Nice, France.

27 Machiels, O., Erpicum, S., Archambeau, P., Dewals, B., & Pirotton, M. (2009, January). Analyse expérimentale du fonctionnement hydraulique des déversoirs en touches de piano. In Conference of the Societé Hydrotechnique de France (SHF) (pp. 20-21).

28 Machiels, O., Erpicum, S., Archambeau, P., Dewals, B., & Pirotton, M. (2009). Large scale experimental study of piano key weirs. In 33rd IAHR Congress. IAHR, Vancouver, Canada.

29 Dewals, B. (2006). Une approche unifiée pour la modélisation d'écoulements à surface libre, de leur effet érosif sur une structure et de leur interaction avec divers constituants.

30 Dewals, B. J., Erpicum, S., Archambeau, P., Detrembleur, S., & Pirotton, M. (2006). Depth-integrated flow modelling taking into account bottom curvature. Journal of Hydraulic Research, 44(6), 785-795.

31 Erpicum, S., Dewals, B., Archambeau, P., Detrembleur, S., & Pirotton, M. (2010). Detailed inundation modelling using high resolution DEMs. Engineering Applications of Computational Fluid Mechanics, 4(2), 196-208.

32 Erpicum, S., Dewals, B. J., Archambeau, P., & Pirotton, M. (2010). Dam break flow computation based on an efficient flux vector splitting. Journal of Computational and Applied Mathematics, 234(7), 2143-2151.

33 Erpicum, S. (2006). Optimisation objective de paramètres en écoulements turbulents à surface libre sur maillage multibloc.

34 Nujić, M. (1995). Efficient implementation of non-oscillatory schemes for the computation of free-surface flows. Journal of Hydraulic Research, 33(1), 101-111.

35 Erpicum, S., Archambeau, P., Dewals, B., & Pirotton, M. (2010). Reliable hydraulic numerical modeling with multiblock grids and linked models.

36 Machiels, O., Erpicum, S., Archambeau, P., Dewals, B., & Pirotton, M. (2010). Hydraulic behavior of Piano Key Weirs: experimental approach. In 3rd Int. Junior Researcher and Engineer Worjshop on Hydraulic Structures.

[037 Machiels, O., Erpicum, S., Archambeau, P., Dewals, B., & Pirotton, M. (2010). Hydraulic behavior of Piano Key Weirs: experimental approach. In 3rd Int. Junior Researcher and Engineer Worjshop on Hydraulic Structures.

38 Machiels, O., Pirotton, M., Pierre, A., Dewals, B., & Erpicum, S. (2014). Experimental parametric study and design of Piano Key Weirs. Journal of Hydraulic Research, 52(3), 326-335.

39 Ribeiro, M. L., Boillat, J. L., Schleiss, A. J., Le Doucen, O., & Laugier, F. (2011, May). Experimental parametric study for hydraulic design of PKWs. In Proc. Int. Conf. Labyrinth and Piano Key Weirs, Liege B (pp. 183-190). CRC Press.

40 Lempérière, F., Vigny, J. P., & Ouamane, A. (2011, May). General comments on Labyrinth and Piano Key Weirs: The past and present. In proceedings of the International Conference Labyrinth and Piano Key Weirs (pp. 17-24).

41 Ouamane, A., & Lempérière, F. (2006, June). Design of a new economic shape of weir. In Proceedings of the International Symposium on Dams in the Societies of the 21st Century (Vol. 18, pp. 463-470).

42 Machiels, O., Erpicum, S., Pirotton, M., Dewals, B., & Archambeau, P. (2012, June). Experimental analysis of PKW hydraulic performance and geometric parameters optimum. In International workshop on Piano Key Weir for In-stream Storage and Dam Safety-PKWISD-2012.

43 Ouamane, A., & Lempérière, F. (2006). Nouvelle conception de déversoir pour l'accroissement de la capacité des retenues des barrages. In Colloque international sur la protection et la préservation des ressources en eau, Bilda, Algérie.

44 Ouamane, A., & Lempérière, F. (2007). Increase of the safety of dams. Rehabilitation of weirs. In ICOLD 75th Annual meeting.